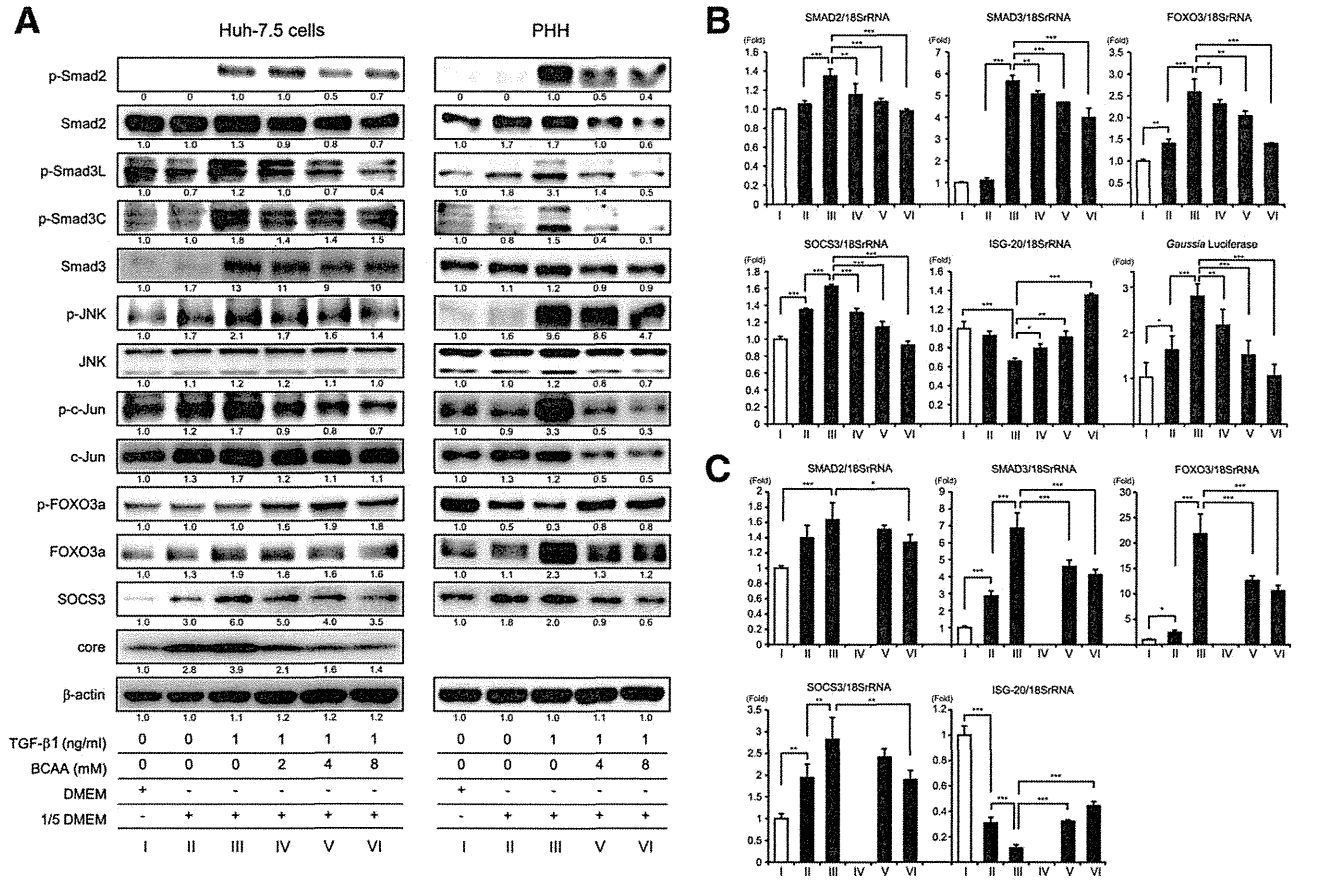

Fig. 7. BCAAs inhibit the effect of malnutrition and TGF-β signaling in Huh-7.5 cells and PHH. A: Western blotting of TGF-β and Foxo3a-Socs3 signaling in Huh-7.5 HCV (+) and PHH treated with amino acid depletion (1/5 DMEM), TGF-β1, and BCAAs. B,C: mRNA expression of TGF-β, Foxo3a-Socs3, and IFN signaling in Huh-7.5 HCV (+) (B) and PHH (C) treated with amino acid depletion (1/5 DMEM), TGF-β1, and BCAA.

blotting analysis showed that BCAAs dose-dependently repressed the expression of p-Smad3L, p-Smad3C, p-JNK, p-c-Jun, Foxo3a, Socs3 (in Huh-7.5 cells and PHH), and HCV core protein (in Huh-7.5 cells), which was induced by amino acid depletion (1/5 DMEM) and TGF-β1 treatment (Fig. 7A). RTD-PCR demonstrated similar mRNA expression patterns (Smad2, Smad3, Foxo3a, and Socs3a) to those obtained by western blotting (Fig. 7B,C), and BCAAs induced the expression of ISG-20 (in Huh-7.5 cells and PHH) and decreased HCV replication in a dose-dependent manner (in Huh-7.5 cells) (Fig. 7B). These results were also confirmed in HCVcc HJ3-5-infected Huh-7 cells (Supporting Fig. 6).

BCAAs and TGF-β RI Potentiate the Anti-HCV Activity of DAAs. Finally, we examined whether BCAAs or TGF-β RI potentiate the anti-HCV activity of DAAs. Amino acid depletion (1/5 DMEM) and TGF-β1 treatment significantly increased HCV replication (deduced from *Gaussia* luciferase activity), and BCAAs (8 mM) and boceprevir (250 nM; NS3 protease inhibitor) inhibited HCV replication to 64% and 50%, respectively (Fig. 8A, black bars). The combination of BCAAs (8 mM) and boceprevir (250 nM) further inhibited HCV replication to 10% and canceled the effect of amino acid depletion (1/5 DMEM) and TGF-β1 treatment, which supported HCV replication (Fig. 8A, compare white and black bars). Similarly, TGF-β RI (10 μM) repressed HCV replication to 60%, and its combination with boceprevir (250 nM) decreased HCV replication to 16% (Fig. 8B, black bars) and canceled the effect of amino acid depletion (1/5 DMEM) and TGF-β1 treatment (Fig. 8A, compare white and black bars). Thus, BCAAs and TGF-β RI had an additive effect on the anti-HCV activity of boceprevir and would be useful for CH-C patients with advanced fibrosis and the IL28B treatment-resistant genotype. A similar effect was obtained by using the NS5A inhibitor BMS-790052; however, its effect was less than that of boceprevir (Supporting Fig. 7).

Discussion

The recently developed DAAs have significantly improved the efficacy of anti-HCV therapy. Triple

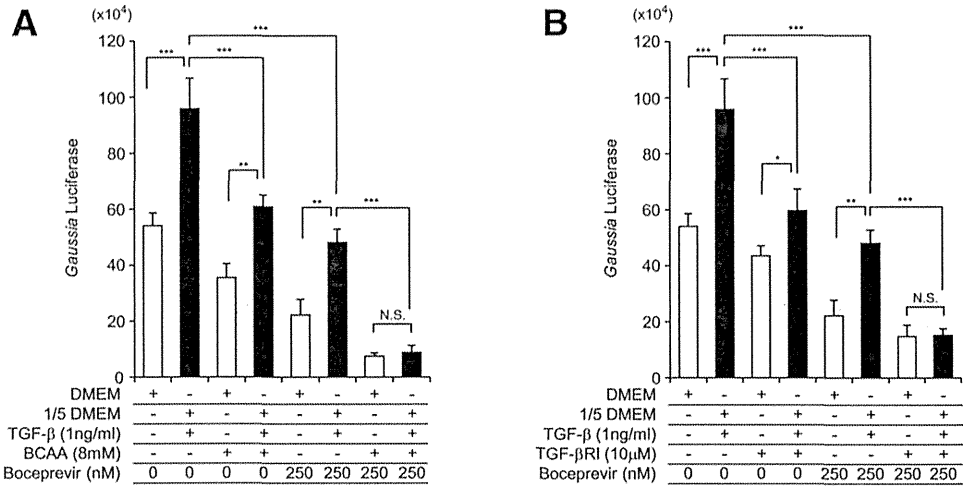

Fig. 8. Anti-HCV activity of boceprevir in combination with BCAAs (A) and TGF-β1 RI (B). HCV replication in Huh-7.5 cells was deduced by *Gaussia* luciferase activity. Boceprevir in combination with BCAAs (A) and TGF-β1 RI (B) efficiently repressed HCV replication in Huh-7.5 cells treated with amino acid depletion (1/5 DMEM) and TGF-β1. The experiments were performed in triplicate and repeated 3 times ($*P < 0.05$, $**P < 0.01$, $***P < 0.001$).

therapy comprising PEG-IFN, RBV, and DAA (e.g., telaprevir or boceprevir) has significantly increased SVR rates; however, its efficacy is poor in difficult-to-cure patients such as those with cirrhosis and the IL28B treatment-resistant genotype.[2,4] An IFN-free regimen using a combination of DAAs would be effective to treat these difficult-to-cure patients; however, the emergence of multiple drug resistant viruses and the high cost of these therapies should be considered carefully in the future. Therefore, standard PEG-IFN plus RBV combination therapy is still useful as an alternative therapy for CH-C.

Previously, we reported that malnutrition in patients with the advanced fibrosis stage of CH-C is associated with IFN resistance and impaired IFN signaling by inhibiting mTORC1 and activating Socs3-mediated IFN inhibitory signaling through the nutrition-sensing transcriptional factor Foxo3a.[6] However, the effect of profibrosis signaling on IFN signaling was not addressed in our previous study. In the present study, using clinical samples and cell lines, we clearly showed that TGF-β signaling inhibits IFN signaling by activating Foxo3a-Socs3-mediated IFN inhibitory signaling (Figs. (1 and 4)) and inhibiting mTORC1 signaling (Fig. 5).

Using Foxo3a promoter-luciferase reporter constructs, we showed that TGF-β1 activated Foxo3a promoter activity through an AP1 transcription factor binding site. Among the components of AP1, c-Jun and probably ATF2, but not c-Fos, were involved in this induction. Previous reports showed that c-Jun and ATF2 were induced by amino acid depletion[13,14] and TGF-β1 treatment,[15,16] although the induction of c-Jun by amino acid depletion was not obvious in PHH in this study. It could be considered that malnutrition and profibrotic signaling cooperatively activated the Foxo3a promoter through the AP1 site and that c-Jun induction was more specifically regulated by TGF-β1 in normal hepatocytes. Mutation of the AP1 binding site (pGL4-FOXO3a [-1340-MT]) abolished the response to amino acid depletion (1/5 DMEM) and TGF-β1 treatment (Fig. 3E; Supporting Fig. 2). Conversely, c-Jun overexpression combined with amino acid depletion (1/5 DMEM) and TGF-β1 treatment activated the Foxo3a promoter by 32-fold (Fig. 3F). In addition, we showed that TGF-β1 inhibited mTORC1 signaling, as demonstrated by the decreased expression of RHEB, p-mTOR, and p-p70S6K (Fig. 5A).

These results were in concordance with gene expression in the liver of CH-C patients. The expression of c-Jun and ATF2 was significantly correlated with Smad2 and Foxo3a expression, respectively (Fig. 4), while the expression of RHEB was significantly negatively correlated with Smad2 expression in the liver of CH-C patients (Fig. 5C). In this study, TGF-β1 and TGF-β2 expression was up-regulated in advanced liver fibrosis, and the expression of TGF-β2 was well correlated with the downstream signaling molecule Smad2 (Fig. 1B-D). Although we could not address the biological differences in TGF-β isoforms in this study, TGF-β1 and TGF-β2 reportedly mediate a similar signaling pathway to induce profibrotic responses.[17] Collectively, TGF-β signaling inhibited IFN signaling by activating Foxo3a-Socs3 IFN inhibitory signaling and

inhibiting mTORC1-IFN stimulating signaling *in vitro* and *in vivo*. Recently, Lee et al. showed that Foxo3a regulates the TGF-β1 promoter directly.[18] Combining their data and ours, there must be positive feedback regulation between TGF-β1 and Foxo3a. Moreover, they identified a polymorphism in Foxo3a (rs12212067: T > G) in which the minor (G) allele was involved in the increased production of TGF-β1 and associated with the inflammatory response.[18] We genotyped the Foxo3a rs12212067 polymorphism in three cell lines and observed TT in Huh-7 and Huh-7.5 and GG in TTNT (Supporting Table 3). Although we could not find a significant difference in Foxo3a promoter activity in response to TGF-β1 among these cell lines (Supporting Fig. 2), further studies should be performed to compare Foxo3a-Socs3 IFN inhibitory signaling among them. Furthermore, it is worthwhile to examine the relationship between the genotype at rs12212067 and treatment response and severity of liver disease in CH-C patients in the future.

Another interesting finding in this study was that TGF-β signaling was related to the IL28B genotype (Fig. 6). The expression of c-Jun was significantly higher in IL28B treatment-resistant minor genotype (TG/GG at rs8099917) patients than in IL28B treatment-sensitive major genotype (TT) patients. Moreover, the expression of c-Jun, Smad2, ATF2, and Socs3 was up-regulated more in IL28B minor genotype patients than in IL28B major genotype patients, especially in those with early stage liver fibrosis (F1-2). The underlying mechanisms of these findings are not known so far; however, we recently reported that the noncanonical WNT signaling ligand WNT5A is up-regulated in the liver of IL28B minor genotype patients and plays a role in treatment resistance.[19] WNT5A reportedly mediates downstream signaling through c-Jun and ATF2 in *Xenopus* cells and human osteosarcoma cells.[20,21] It could be speculated that WNT5A potentiates TGF-β signaling through these transcription factors, although this hypothesis should be tested in the future.

We examined whether BCAAs and TGF-β RI improve the IFN inhibitory signaling induced by malnutrition and TGF-β signaling (Fig. 7). Previously, we demonstrated that BCAAs improved the IFN signaling that was inhibited by malnutrition.[6] In the present study, we found that BCAAs blocked TGF-β signaling by decreasing the levels of p-Smad3L, p-JNK, and c-Jun (Fig. 7A). Consequently, BCAAs decreased the expression of Foxo3a, Socs3, and HCV core protein (Fig. 7). In addition, we found that the combination of BCAAs or TGF-β RI and the NS3 protease inhibitor boceprevir efficiently inhibited HCV replication and canceled the positive effects of malnutrition and TGF-β1 on HCV replication (Fig. 8). A recent report showed that the NS3 protease of HCV mimics TGF-β2 and activates the TGF-β type I receptor.[22] Therefore, the anti-HCV effect of boceprevir could be potentiated in combination with BCAAs or TGF-β RI, which blocked TGF-β signaling and increased IFN signaling. Therefore, the combination of BCAAs or TGF-β RI with DAAs could be useful for the treatment of difficult-to-cure CH-C patients with advanced liver fibrosis and the IL28B treatment-resistant genotype.

In conclusion, we clarified that TGF-β signaling inhibits IFN signaling and is related to the treatment-resistant phenotype of CH-C patients with advanced liver fibrosis and the IL28B treatment-resistant genotype. Furthermore, blocking TGF-β signaling by BCAAs or TGF-β RI could potentiate the anti-HCV effect of DAAs. An oral TGF-β RI small compound, LY2157299, is now being assessed in a phase II trial for the treatment of advanced-stage HCC. Further studies should be performed to address the significance of these compounds for the eradication of HCV in patients with advanced liver fibrosis for preventing HCC.

Acknowledgment: The authors thank Mina Nishiyama for technical assistance.

Author Contributions: Takayoshi Shirasaki performed most experiments and drafted the article; Masao Honda, study design, interpretation of data, and drafting of the article; Tetsuro Shimakami, HCV replication analysis and cellular experiments; Kazuhisa Murai, HCV replication analysis and cellular experiments; Takayuki Shiomoto, HCV replication analysis and cellular experiments; Hikari Okada, HCV replication analysis and cellular experiments; Riuta Takabatake, HCV replication analysis and cellular experiments; Akihiro Tokumaru, HCV replication analysis and cellular experiments; Yoshio Sakai, acquisition of clinical data; Taro Yamashita, acquisition of clinical data; Stanley M. Lemon, study design and interpretation of data; Seishi Murakami, study design and interpretation of data; Shuichi Kaneko, study concept and design.

References

1. Yoshida H, Shiratori Y, Moriyama M, Arakawa Y, Ide T, Sata M, et al. Interferon therapy reduces the risk for hepatocellular carcinoma: national surveillance program of cirrhotic and noncirrhotic patients with chronic hepatitis C in Japan IHIT Study Group. Inhibition of Hepatocarcinogenesis by Interferon Therapy. Ann Intern Med 1999;131:174-181.

2. Trembling PM, Tanwar S, Rosenberg WM, Dusheiko GM. Treatment decisions and contemporary versus pending treatments for hepatitis C. Nat Rev Gastroenterol Hepatol 2013;10:713-728.
3. Hezode C, Fontaine H, Dorival C, Larrey D, Zoulim F, Canva V, et al. Triple therapy in treatment-experienced patients with HCV-cirrhosis in a multicentre cohort of the French Early Access Programme (ANRS CO20-CUPIC) – NCT01514890. J Hepatol 2013;59:434-441.
4. Bruno S, Vierling JM, Esteban R, Nyberg LM, Tanno H, Goodman Z, et al. Efficacy and safety of boceprevir plus peginterferon-ribavirin in patients with HCV G1 infection and advanced fibrosis/cirrhosis. J Hepatol 2013;58:479-487.
5. Tanaka Y, Nishida N, Sugiyama M, Kurosaki M, Matsuura K, Sakamoto N, et al. Genome-wide association of IL28B with response to pegylated interferon-alpha and ribavirin therapy for chronic hepatitis C. Nat Genet 2009;41:1105-1109.
6. Honda M, Takehana K, Sakai A, Tagata Y, Shirasaki T, Nishitani S, et al. Malnutrition impairs interferon signaling through mTOR and FoxO pathways in patients with chronic hepatitis C. Gastroenterology 2011;141:128-140.
7. Okitsu T, Kobayashi N, Jun HS, Shin S, Kim SJ, Han J, et al. Transplantation of reversibly immortalized insulin-secreting human hepatocytes controls diabetes in pancreatectomized pigs. Diabetes 2004;53:105-112.
8. Honda M, Nakamura M, Tateno M, Sakai A, Shimakami T, Shirasaki T, et al. Differential interferon signaling in liver lobule and portal area cells under treatment for chronic hepatitis C. J Hepatol 2010;53:817-826.
9. Yi M, Ma Y, Yates J, Lemon SM. Compensatory mutations in E1, p7, NS2, and NS3 enhance yields of cell culture-infectious intergenotypic chimeric hepatitis C virus. J Virol 2007;81:629-638.
10. Eferl R, Wagner EF. AP-1: a double-edged sword in tumorigenesis. Nat Rev Cancer 2003;3:859-868.
11. Bai X, Ma D, Liu A, Shen X, Wang QJ, Liu Y, et al. Rheb activates mTOR by antagonizing its endogenous inhibitor, FKBP38. Science 2007;318:977-980.
12. Carayol N, Katsoulidis E, Sassano A, Altman JK, Druker BJ, Platanias LC. Suppression of programmed cell death 4 (PDCD4) protein expression by BCR-ABL-regulated engagement of the mTOR/p70 S6 kinase pathway. J Biol Chem 2008;283:8601-8610.
13. Chaveroux C, Jousse C, Cherasse Y, Maurin AC, Parry L, Carraro V, et al. Identification of a novel amino acid response pathway triggering ATF2 phosphorylation in mammals. Mol Cell Biol 2009;29:6515-6526.
14. Fu L, Balasubramanian M, Shan J, Dudenhausen EE, Kilberg MS. Auto-activation of c-JUN gene by amino acid deprivation of hepatocellular carcinoma cells reveals a novel c-JUN-mediated signaling pathway. J Biol Chem 2011;286:36724-36738.
15. Sano Y, Harada J, Tashiro S, Gotoh-Mandeville R, Maekawa T, Ishii S. ATF-2 is a common nuclear target of Smad and TAK1 pathways in transforming growth factor-beta signaling. J Biol Chem 1999;274:8949-8957.
16. Mu Y, Gudey SK, Landstrom M. Non-Smad signaling pathways. Cell Tissue Res 2012;347:11-20.
17. Leask A, Abraham DJ. TGF-beta signaling and the fibrotic response. FASEB J 2004;18:816-827.
18. Lee JC, Espeli M, Anderson CA, Linterman MA, Pocock JM, Williams NJ, et al. Human SNP links differential outcomes in inflammatory and infectious disease to a FOXO3-regulated pathway. Cell 2013;155:57-69.
19. Honda M, Shirasaki T, Shimakami T, Sakai A, Horii R, Arai K, et al. Hepatic interferon-stimulated genes are differentially regulated in the liver of chronic hepatitis C patients with different interleukin 28B genotypes. HEPATOLOGY 2014;59:828-838.
20. Yamanaka H, Moriguchi T, Masuyama N, Kusakabe M, Hanafusa H, Takada R, et al. JNK functions in the non-canonical Wnt pathway to regulate convergent extension movements in vertebrates. EMBO Rep 2002;3:69-75.
21. Yamagata K, Li X, Ikegaki S, Oneyama C, Okada M, Nishita M, et al. Dissection of Wnt5a-Ror2 signaling leading to matrix metalloproteinase (MMP-13) expression. J Biol Chem 2012;287:1588-1599.
22. Sakata K, Hara M, Terada T, Watanabe N, Takaya D, Yaguchi S, et al. HCV NS3 protease enhances liver fibrosis via binding to and activating TGF-beta type I receptor. Sci Rep 2013;3:3243.

Supporting Information

Additional Supporting Information may be found in the online version of this article at the publisher's website.

nature medicine

Regulation of the hepatitis C virus RNA replicase by endogenous lipid peroxidation

Daisuke Yamane[1,2], David R McGivern[1,2], Eliane Wauthier[2,3], MinKyung Yi[4], Victoria J Madden[5], Christoph Welsch[6], Iris Antes[7], Yahong Wen[8], Pauline E Chugh[2,9], Charles E McGee[10], Douglas G Widman[11], Ichiro Misumi[10], Sibali Bandyopadhyay[12,13], Seungtaek Kim[1,2,14], Tetsuro Shimakami[1,2], Tsunekazu Oikawa[2,3], Jason K Whitmire[2,9,10], Mark T Heise[2,10], Dirk P Dittmer[2,9], C Cheng Kao[8], Stuart M Pitson[15], Alfred H Merrill Jr[12,13], Lola M Reid[2,3] & Stanley M Lemon[1,2,9]

Oxidative tissue injury often accompanies viral infection, yet there is little understanding of how it influences virus replication. We show that multiple hepatitis C virus (HCV) genotypes are exquisitely sensitive to oxidative membrane damage, a property distinguishing them from other pathogenic RNA viruses. Lipid peroxidation, regulated in part through sphingosine kinase-2, severely restricts HCV replication in Huh-7 cells and primary human hepatoblasts. Endogenous oxidative membrane damage lowers the 50% effective concentration of direct-acting antivirals *in vitro*, suggesting critical regulation of the conformation of the NS3-4A protease and the NS5B polymerase, membrane-bound HCV replicase components. Resistance to lipid peroxidation maps genetically to transmembrane and membrane-proximal residues within these proteins and is essential for robust replication in cell culture, as exemplified by the atypical JFH1 strain of HCV. Thus, the typical, wild-type HCV replicase is uniquely regulated by lipid peroxidation, providing a mechanism for attenuating replication in stressed tissue and possibly facilitating long-term viral persistence.

Reactive oxygen species (ROS) are an unavoidable byproduct of aerobic metabolism and a double-edged sword for complex cellular systems[1]. Although central to many disease states, ROS also function as second messengers during embryonic development and, in macrophages, contribute to host defense against infection[2,3]. Viral infections frequently induce ROS generation, either by stimulating host immune responses or by direct tissue injury[4]. HCV, a hepatotropic RNA virus with a unique capacity for persistence[5], induces substantial intrahepatic oxidative stress, thereby promoting liver injury[6,7]. Limited data suggest that lipid peroxidation restricts HCV replication[8], but how it impairs the viral replicative machinery is unknown.

Although HCV is a leading cause of cirrhosis and liver cancer[5], many details of its replication remain obscure, as most HCV strains replicate poorly in cell culture. A notable exception is JFH1, a genotype 2a virus recovered from a patient with fulminant hepatitis[9]. JFH1 recapitulates the entire virus life cycle and replicates efficiently in Huh-7 hepatoma cells[9–11]. In recent years, it has become a laboratory standard used in most studies of HCV replication. However, there is very limited understanding of the robust replication phenotype that sets it apart from other HCVs[12,13].

Like all positive-strand RNA virus genomes, the HCV genome is synthesized by a multiprotein replicase complex that assembles in association with intracellular membranes. Known as the 'membranous web' in HCV-infected cells[14,15], this specialized cytoplasmic compartment provides a platform for viral RNA synthesis. Its membranes are enriched in cholesterol, sphingolipids and phosphatidylinositol-4-phosphate[16,17]. Assembly of the membranous web involves recruitment of phosphatidylinositol-4-phosphate-3 kinase and annexin A2 (refs. 17–19) and possibly also direct membrane remodeling by nonstructural HCV proteins[20]. Whereas lipid metabolism also plays key roles in later steps in the virus life cycle[21], these modifications of intracellular membranes are closely linked to viral RNA synthesis.

Sphingolipids are increased in abundance within the replicase membranes and are important factors in HCV replication[22–25]. Sphingomyelin interacts with and in some genotypes stimulates NS5B, the viral RNA-dependent RNA polymerase[23,26]. While studying

[1]Department of Medicine, Division of Infectious Diseases, The University of North Carolina at Chapel Hill, Chapel Hill, North Carolina, USA. [2]Lineberger Comprehensive Cancer Center, The University of North Carolina at Chapel Hill, Chapel Hill, North Carolina, USA. [3]Department of Cell Biology and Physiology, The University of North Carolina at Chapel Hill, Chapel Hill, North Carolina, USA. [4]Department of Microbiology and Immunology, University of Texas Medical Branch, Galveston, Texas, USA. [5]Department of Pathology, The University of North Carolina at Chapel Hill, Chapel Hill, North Carolina, USA. [6]Department of Internal Medicine I, J.W. Goethe University Hospital, Frankfurt, Germany. [7]Center for Integrated Protein Science Munich (CIPSM), Department of Life Sciences, Technical University Munich, Freising, Germany. [8]Department of Molecular and Cellular Biochemistry, Indiana University, Bloomington, Indiana, USA. [9]Department of Microbiology and Immunology, The University of North Carolina at Chapel Hill, Chapel Hill, North Carolina, USA. [10]Department of Genetics, The University of North Carolina at Chapel Hill, Chapel Hill, North Carolina, USA. [11]Department of Epidemiology, The University of North Carolina at Chapel Hill, Chapel Hill, North Carolina, USA. [12]School of Biology, Georgia Institute of Technology, Atlanta, Georgia, USA. [13]Parker H. Petit Institute for Bioengineering and Bioscience, Georgia Institute of Technology, Atlanta, Georgia, USA. [14]Severance Biomedical Science Institute, Yonsei University College of Medicine, Seoul, Korea. [15]Centre for Cancer Biology, SA Pathology, Adelaide, South Australia, Australia. Correspondence should be addressed to D.Y. (yamane@email.unc.edu) or S.M.L. (smlemon@med.unc.edu).

Received 31 March; accepted 23 May; published online 27 July 2014; doi:10.1038/nm.3610

these virus-host interactions in cell culture, we discovered that JFH1 differs from other HCV strains in its response to inhibitors of sphingolipid-converting enzymes. These initial observations led to experiments that show the HCV replicase to be exquisitely sensitive to endogenous lipid peroxidation, a feature lacking in the atypical JFH1 strain and other pathogenic RNA viruses. Our findings suggest that HCV possesses a unique capacity to sense lipid peroxides induced by infection and to respond to their presence by restricting viral RNA synthesis, thereby limiting virus replication and possibly facilitating virus persistence.

RESULTS

Sphingosine kinase-2 regulates HCV replication

We determined how inhibitors of sphingolipid-converting enzymes influence replication of three cell culture–adapted HCVs: H77S.3, a genotype 1a virus, N2, a genotype 1b virus, and HJ3-5, an intergenotypic chimera expressing the genotype 2a JFH1 replicase. To assess replication, we monitored *Gaussia princeps* luciferase (GLuc) produced by Huh-7.5 cells transfected with synthetic viral RNAs containing in-frame GLuc insertions[27] (**Fig. 1a**). Unexpectedly, the H77S.3/GLuc and HJ3-5/GLuc RNAs demonstrated contrary responses to many inhibitors, including, most notably, SKI, a sphingosine kinase (SPHK) inhibitor (**Fig. 1b** and **Supplementary Fig. 1a,b**). We also observed contrasting responses to sphingolipid supplementation (**Supplementary Fig. 1c**). SKI (1 μM) enhanced replication of H77S.3/GLuc and also N.2/GLuc by three- to sixfold but suppressed replication of HJ3-5/GLuc (**Fig. 1b,c**). These effects were evident within 48 h of exposure. We observed similar effects with viral RNAs lacking GLuc insertions: SKI enhanced H77S.3 protein expression tenfold while slightly suppressing HJ3-5 protein expression (**Fig. 1d**). Thus, changes in the cellular environment induced by SKI favor H77S.3 and N.2 replication and inhibit that of HJ3-5. These effects were not due to altered cell proliferation or viral RNA translation (**Supplementary Fig. 2a,b**). We observed similar results with autonomously replicating, subgenomic HCV RNAs ('replicons') in multiple cell types (**Supplementary Fig. 2c,d**).

SPHK is expressed as two isoforms[28], which we individually silenced by transfecting cells with gene-specific siRNAs. Partial type 2 SPHK (SPHK2) depletion enhanced replication of H77S.3/GLuc and N.2/GLuc, whereas SPHK1 depletion inhibited both viruses (**Fig. 1e,f**). In contrast, replication of HJ3-5/GLuc and cell culture–adapted JFH1 (JFH-QL/GLuc, **Fig. 1a**) viruses was increased following SPHK1 depletion and decreased after SPHK2 knockdown. Neither SPHK1 nor SPHK2 knockdown substantially affected cell proliferation (**Supplementary Fig. 2e**). Thus, SKI enhances replication of H77S.3/GLuc and N.2/GLuc by inhibiting SPHK2. Consistent with this, SKI preferentially inhibited SPHK2 in cell-free assays (**Supplementary Fig. 2f**) and demonstrated no activity against endogenous SPHK1 at low concentrations (≤2 μM) (**Supplementary Fig. 2g**). SKI did not act by regulating the intracellular abundance of sphingomyelin, cholesterol, triglyceride or lipid droplets, and sensitivity to SKI was not determined by the sphingomyelin binding domain of NS5B (**Supplementary Results** and **Supplementary Figs. 3** and **4**).

Lipid peroxidation is a key factor in SKI regulation of HCV

Polyunsaturated fatty acids (PUFAs) inhibit replication of genotype 1b HCV replicons by inducing lipid peroxidation[8,29]. Notably, although PUFAs such as arachidonic acid, docosahexaenoic acid or linoleic acid potently suppressed H77S.3/GLuc replication without affecting cell viability, HJ3-5/GLuc was highly resistant to this inhibitory effect (**Fig. 2a,b** and **Supplementary Fig. 5a,b**). Thus, PUFAs appear to phenocopy the effect of SPHK2 on HCV replication, suggesting that SPHK2 promotes lipid peroxidation. Consistent with this hypothesis, SKI completely abolished the inhibitory effects of PUFAs on H77S.3/GLuc and N.2/GLuc (**Fig. 2c**). SKI also lowered the intracellular abundance of malondialdehyde (MDA), a secondary product

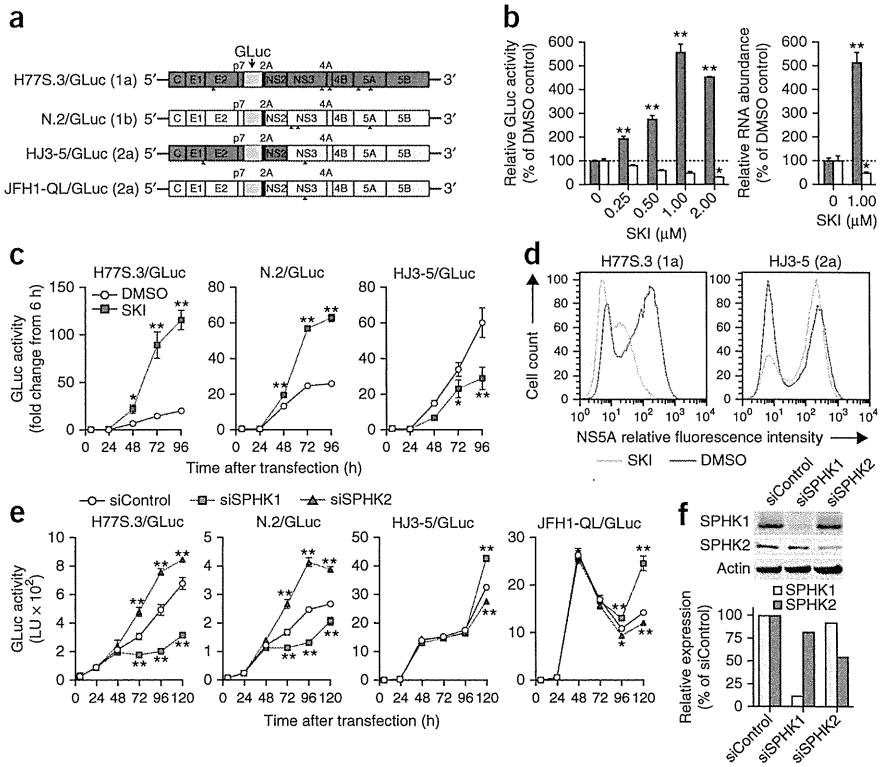

Figure 1 SKI enhances genotype 1 HCV replication while suppressing JFH1-based viruses by inhibiting SPHK2. (**a**) HCV RNA genomes that express GLuc fused to foot-and-mouth disease virus 2A autoprotease as part of the HCV polyprotein. Arrowheads indicate cell culture–adaptive mutations. (**b**) Left, dose-response effects of SKI on replication of H77S.3/GLuc (red) or HJ3-5/GLuc (blue) RNAs in Huh-7.5 cells. Right, effect of 1 μM SKI on replication of H77S.3 (red) or HJ3-5 (blue) RNAs. Data represent relative amounts of GLuc secreted between 48–72 h (left) or intracellular RNA levels at 72 h (right). $*P < 0.05$, $**P < 0.001$ by two-way ANOVA. (**c**) Effect of 1 μM SKI on GLuc activities of the indicated viruses presented as fold change from baseline (6 h). $*P < 0.05$, $**P < 0.001$ by two-way ANOVA. (**d**) Flow cytometric analysis of NS5A expression in Huh-7.5 cells electroporated with H77S.3 or HJ3-5 RNA and treated with 1 μM SKI or DMSO. (**e**,**f**) Effect of siRNAs targeting SPHK isoforms or nontargeting control siRNA on replication of different HCV RNAs (**e**) and protein abundance of each SPHK isoform (**f**). LU, light units. $*P < 0.05$, $**P < 0.01$ by two-way ANOVA. Results represent the mean ± s.e.m. from two independent (**b**,**c**,**d**) or triplicate (**e**) experiments.

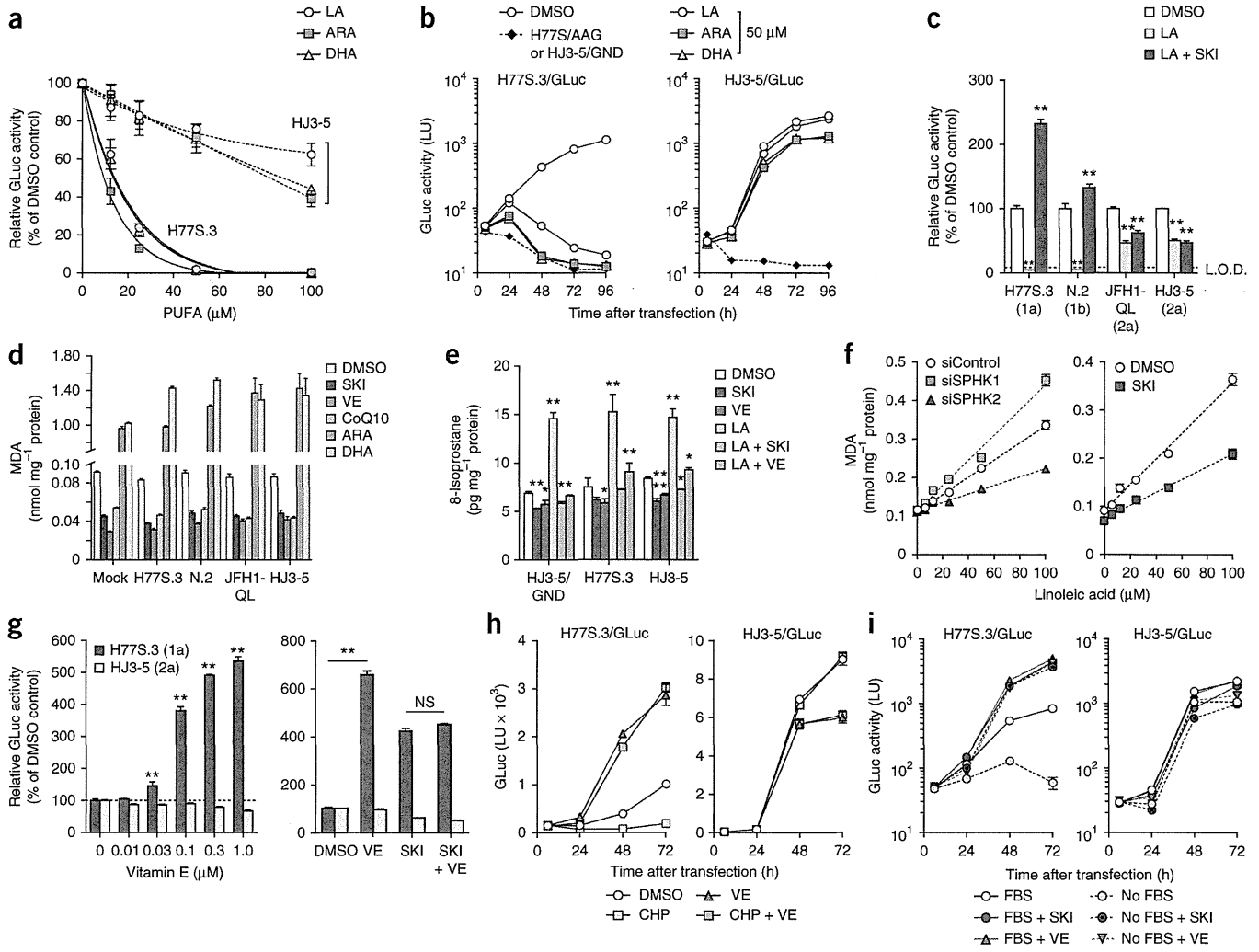

Figure 2 Differential regulation of HCV strains by SPHK2-mediated lipid peroxidation. (**a**) Dose-dependent effects of PUFAs on H77S.3/GLuc and HJ3-5/GLuc RNAs in Huh-7.5 cells. Data represent percentage secreted GLuc activity between 48–72 h relative to DMSO control. (**b**) Growth kinetics of H77S.3/GLuc and HJ3-5/GLuc RNAs in the presence of 50 μM PUFAs. Data are mean ± s.e.m. of GLuc activity in supernatant fluids of two replicate cultures. (**c**) Cells transfected with HCV RNAs encoding GLuc treated with DMSO, 100 μM linoleic acid (LA) or 100 μM linoleic acid plus 1 μM SKI. Data represent percentage secreted GLuc activity between 48–72 h relative to DMSO control. L.O.D., limit of detection. (**d**) Effect of 1 μM SKI, 1 μM vitamin E (VE), 100 μM CoQ10 or 50 μM arachidonic acid (ARA) or docosahexaenoic acid (DHA) on intracellular MDA abundance in cells transfected with the indicated HCV/GLuc RNAs at 72 h. MDA was significantly increased by PUFAs and reduced by SKI or lipophilic antioxidants ($P < 0.01$ by ANOVA). (**e**) Analysis of 8-isoprostane abundance in cells electroporated with the indicated HCV RNAs and grown in the presence of 1 μM SKI or vitamin E or of 50 μM linoleic acid with or without 1 μM SKI or vitamin E for 48 h. (**f**) Left, effect of siRNA targeting SPHK isoforms (**Fig. 1f**) on MDA accumulation after treatment with increasing concentrations of linoleic acid (6.25, 12.5, 25, 50, 100 μM) for 24 h. Right, MDA levels in Huh-7.5 cells treated with increasing concentrations of linoleic acid in the presence of DMSO or 1 μM SKI. (**g**) Effects of increasing concentrations of vitamin E (left) or 1 μM vitamin E alone or 1 μM vitamin E plus 1 μM SKI (right) on replication of H77S.3/GLuc and HJ3-5/GLuc RNAs. Data represent GLuc secreted between 48–72 h relative to DMSO control. NS, not significant. (**h**) GLuc secretion from Huh-7.5 cells transfected as in **a** and treated with 10 μM CHP with or without 10 μM vitamin E. (**i**) Influence of SKI or vitamin E (each 1 μM) on replication of H77S.3 and HJ3-5 viruses expressing GLuc in cells cultured in the presence or absence of 10% FBS. Data represent mean ± s.e.m. from two (**a–f,i**) or three (**g,h**) independent experiments. $^*P < 0.05$, $^{**}P < 0.01$ by two-way ANOVA.

of peroxidative degradation, in both HCV-infected and uninfected cells (**Fig. 2d**). SKI was as effective as the lipophilic antioxidants vitamin E (α-tocopherol) and coenzyme Q10 (CoQ10) in reducing MDA abundance and, like vitamin E and CoQ10, prevented large increases in lipid peroxidation induced by PUFAs (**Fig. 2d,e**). SKI also reduced both endogenous and PUFA-induced synthesis of 8-isoprostane, an alternative biomarker of lipid peroxidation (**Fig. 2e**). Conversely, RNAi-mediated depletion of SPHK1 increased the intracellular abundance of MDA in cells treated with increasing concentrations of linoleic acid, whereas SPHK2 knockdown, like SKI, reduced it (**Fig. 2f**). Thus, the contrasting effects of SPHK1 and SPHK2 on HCV replication may be explained by their opposing actions on peroxidation of endogenous PUFA. These results identify SPHK2 as a key mediator of lipid peroxidation.

Lipid-soluble antioxidants, including multiple forms of vitamin E (α-, *rac*-β- and γ-tocopherols), CoQ10 and butylated hydroxytoluene, enhanced H77S.3/GLuc replication in a concentration-dependent fashion, as described for a genotype 1b replicon[8], but suppressed HJ3-5/GLuc replication (**Fig. 2g** and **Supplementary Fig. 5c–e**). Notably, the effects of vitamin E and SKI on H77S.3/GLuc or N.2/GLuc replication were not additive (**Fig. 2g** and **Supplementary Fig. 5f**), suggesting

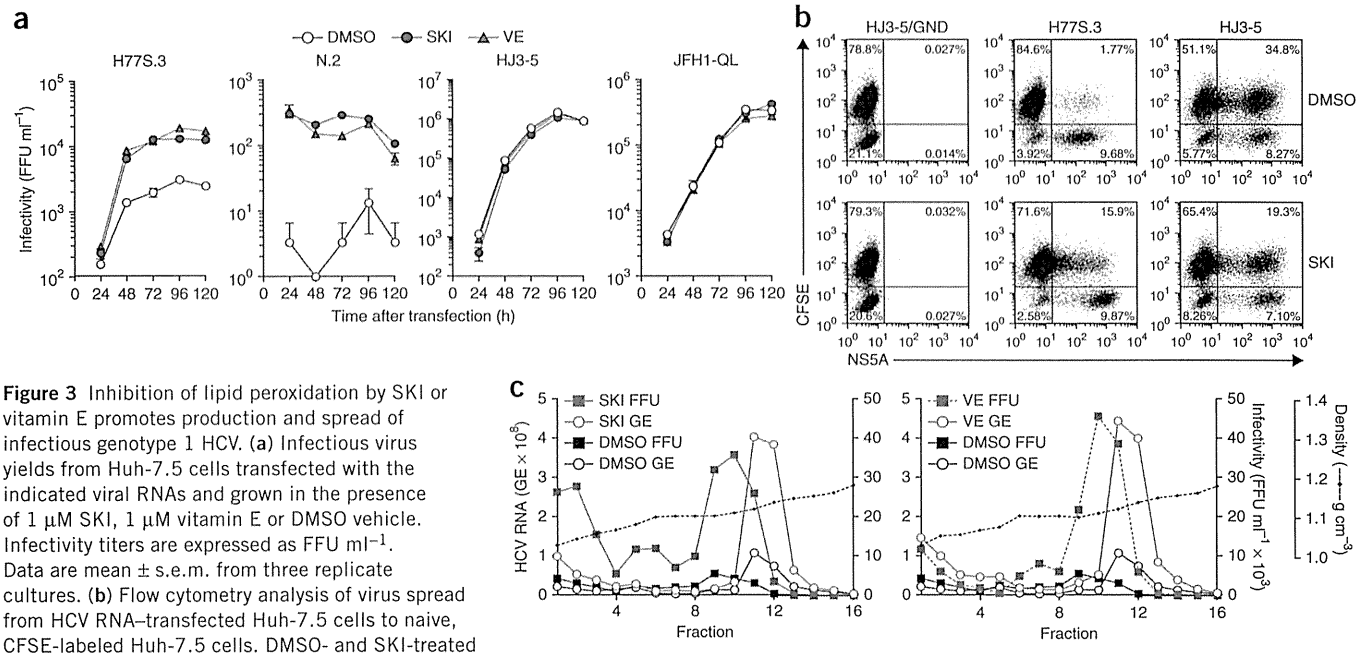

Figure 3 Inhibition of lipid peroxidation by SKI or vitamin E promotes production and spread of infectious genotype 1 HCV. (**a**) Infectious virus yields from Huh-7.5 cells transfected with the indicated viral RNAs and grown in the presence of 1 μM SKI, 1 μM vitamin E or DMSO vehicle. Infectivity titers are expressed as FFU ml^{-1}. Data are mean ± s.e.m. from three replicate cultures. (**b**) Flow cytometry analysis of virus spread from HCV RNA–transfected Huh-7.5 cells to naive, CFSE-labeled Huh-7.5 cells. DMSO- and SKI-treated cultures are shown for each transfected RNA. Percentages represent the percentage of all cells in each quadrant. $CFSE^+NS5A^+$ cells (upper right quadrant) are indicative of virus spread. (**c**) Buoyant density of H77S.3 virus particles released from H77S.3 RNA–transfected Huh-7.5 cells grown in 1 μM SKI (left) or 1 μM vitamin E (right) versus DMSO control. Fractions from isopycnic iodixanol gradients were assayed for infectious virus (FFU) or HCV RNA (GE, genome equivalents). Data are representative of two independent experiments.

that both act via a common antioxidant mechanism. Antioxidants that are not soluble in lipids, such as ebselen and *N*-acetylcysteine, as well as the NADPH oxidase inhibitor diphenyleneiodonium, had very little effect on H77S.3/GLuc replication (**Supplementary Fig. 5g**), whereas cumene hydroperoxide (CHP), a lipophilic oxidant, suppressed H77S.3/GLuc replication in a vitamin E–reversible fashion (**Fig. 2h**). FBS contains substantial quantities of lipophilic antioxidants[8]. H77S.3/GLuc replication was 20-fold lower in FBS-free cultures but was enhanced 100-fold with either SKI or vitamin E (**Fig. 2i**). HJ3-5/GLuc replication was relatively unimpaired in FBS-free medium. Collectively, these data provide evidence that endogenous lipid peroxidation restricts H77S.3/GLuc and N.2/GLuc replication, whereas the JFH1 replicase is resistant to both endogenous and chemically induced lipid peroxidation.

Endogenous lipid peroxidation restricts infectious HCV yield

Both SKI and vitamin E induced a tenfold increase in the yield of infectious virus released by H77S.3 RNA–transfected cells, reaching ~20,000 focus-forming units per milliliter (FFU ml^{-1}) (**Fig. 3a** and **Supplementary Fig. 6a**). Infectious N.2 virus yields were increased up to 100-fold (**Fig. 3a**). SKI also enhanced virus spread when we cultured H77S.3 RNA–transfected cells with nontransfected carboxyfluorescein succinimidyl ester (CFSE)-labeled cells (**Fig. 3b**). In contrast, neither SKI nor vitamin E enhanced infectious yields of JFH1-QL or HJ3-5 viruses (**Fig. 3a**), whereas SKI reduced the spread of HJ3-5 virus by >40% (**Fig. 3b**).

HCV particles produced in cell culture have heterogeneous buoyant densities[30]. However, most H77S.3 particles produced in the absence of SKI or vitamin E banded between 1.12 and 1.14 g cm^{-3} in isopycnic gradients, with peak infectivity banding between 1.10 and 1.11 g cm^{-3} (**Fig. 3c**). Neither SKI nor vitamin E altered the distribution of RNA-containing or infectious particles in gradients, but they substantially increased the abundance of both (**Fig. 3c**). SKI and vitamin E also caused modest increases in the maximum specific infectivity of virus particles (**Supplementary Fig. 6b**). Thus, SKI and vitamin E act primarily on replication of H77S.3 RNA, leading to enhanced production of infectious virus.

Lipid peroxidation restricts HCV in primary hepatocytes

To assess replication of wild-type HCV genomes possessing no cell culture–adaptive mutations, we inserted a GLuc sequence into infectious molecular clones of H77c and N[31,32]. Both H77c/GLuc and N/GLuc RNAs produced more GLuc in electroporated cells than RNA with a lethal mutation in NS5B, H77c/GLuc-AAG (**Fig. 4a**). GLuc secretion produced by either RNA was eliminated by direct-acting antivirals (DAA) targeting NS5B, confirming it represents genuine viral replication. Treatment with either SKI or vitamin E markedly increased GLuc production, whereas linoleic acid decreased GLuc secretion to background (**Fig. 4a**). Moreover, the inhibitory effect of linoleic acid was reversed by cotreatment with SKI or vitamin E. In contrast, GLuc production by wild-type JFH1/GLuc was not affected by SKI, vitamin E or linoleic acid (**Fig. 4b**). Thus, endogenous lipid peroxidation is a critical restriction factor for H77c and N viruses but not for wild-type JFH1.

To assess the effects of SKI and vitamin E on HCV replication in cells that are closely related to those naturally infected by the virus, we studied primary human fetal hepatoblasts (HFHs). SKI and vitamin E significantly increased replication of the H77S.3/GLuc reporter virus in HFHs ($P < 0.0001$ by two-way analysis of variance (ANOVA) with Holm-Sidak correction for multiple comparisons), sustaining GLuc expression for 7 d after low-multiplicity infection (**Fig. 4c,d**). In contrast, linoleic acid suppressed H77S.3 infection in HFHs in a vitamin E–reversible manner (**Fig. 4d**). Whereas H77S.3/GLuc replicated efficiently in the presence of vitamin E or SKI, HJ3-5/GLuc replication was inhibited by SKI ($P < 0.001$ by two-way ANOVA with Holm-Sidak correction for multiple comparisons) and to a lesser extent by vitamin E

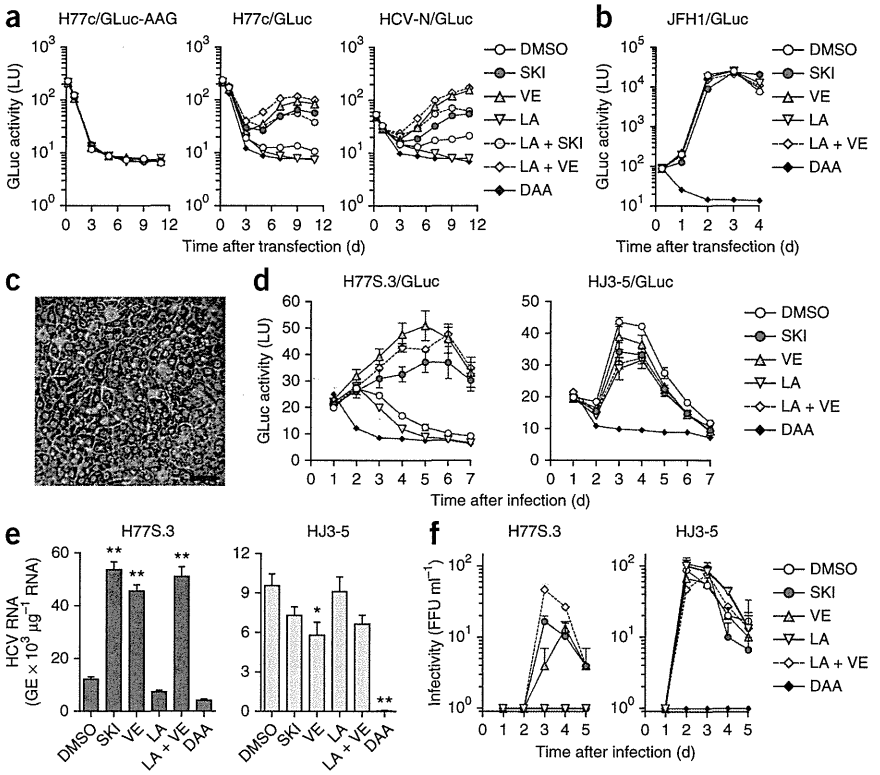

Figure 4 Lipid peroxidation regulates wild-type HCV replication and represses cell culture–adapted virus in primary human liver cultures. (**a**) Effects of SKI or vitamin E (each 1 μM), linoleic acid (20 μM), linoleic acid + SKI, linoleic acid + vitamin E or a DAA (MK-0608, 10 μM) on replication of wild-type H77c/GLuc or HCV-N/GLuc RNAs or a replication-defective control (H77c/GLuc-AAG) in Huh-7.5 cells. (**b**) Effects of SKI, vitamin E and linoleic acid (as in **a**) on replication of wild-type JFH1/GLuc RNA. DAA, PSI-6130 (10 μM). (**c**) Phase contrast microscopy of fetal hepatoblasts at 3 d. Scale bar, 50 μm. (**d**) HFHs infected with H77S.3/GLuc or HJ3-5/GLuc viruses (multiplicity of infection (MOI) = 0.001) in HFH medium containing SKI or vitamin E (each 1 μM), linoleic acid (50 μM), linoleic acid + vitamin E or a DAA (MK-0608 or PSI-6130, 10 μM) and assayed for GLuc. Results represent mean ± s.e.m. from three replicate cultures with cells from two donors. $P < 0.0001$ for SKI, VE and LA + VE compared to DMSO at 5–7 d, two-way ANOVA with Holm-Sidak correction for multiple comparisons. (**e**) HFHs infected with H77S.3 or HJ3-5 (MOI = 0.01) and treated as in **d**. Cell-associated viral RNA was quantified by quantitative RT-PCR (qRT-PCR) at 5 d (*$P < 0.05$, **$P < 0.001$ by two-way ANOVA. GE, genome equivalent. (**f**) Infectious virus released from H77S.3 or HJ3-5 virus–inoculated HFHs (MOI = 0.01). Virus was quantified by FFU assay. Results represent mean ± s.e.m. from three replicate cultures.

($P < 0.05$) (**Fig. 4d**). We observed similar results in cells infected with H77S.3 or HJ3-5 viruses lacking a GLuc insertion (**Fig. 4e**). We detected production of infectious H77S.3 virus in HFH cultures only in the presence of vitamin E or SKI and found that infectious HJ3-5 yields were not enhanced by either treatment (**Fig. 4f**). Whereas the disruption of innate immune responses is known to promote HCV replication in HFHs[33], neither SKI nor vitamin E reduced Sendai virus activation of the interferon-β promoter (**Supplementary Fig. 7**). Thus, SKI and vitamin E do not promote H77S.3 replication in HFHs by blocking activation of the interferon response to virus infection.

Lipid peroxidation reduces the EC_{50} of direct antivirals

Both SKI and vitamin E treatment increased the area occupied by the membranous web in H77S.3-infected cells (**Fig. 5a,b**) without altering the morphology of double-membrane vesicles, which are the likely site of genome replication[14]. Increased lipid peroxidation reduced the area occupied by the membranous web, whereas the HJ3-5 membranous web was insensitive to changes in lipid peroxidation.

Reverse molecular genetic studies involving exchanges between the H77S.3 and JFH1 genomes suggested that the peroxidation resistance phenotype of JFH1 involves multiple nonstructural proteins within the replicase (**Supplementary Results** and **Supplementary Fig. 8**). Consistent with this, we observed an unexpected increase in the 50% effective concentration (EC_{50}) of DAAs targeting the NS3-4A protease (a noncovalent complex of NS3 and its cofactor, NS4A) and NS5B polymerase after suppressing endogenous lipid peroxidation in H77S.3/GLuc-infected cells (**Fig. 5d,e** and **Supplementary Fig. 9a–c**). Both SKI and vitamin E masked the antiviral effects of PSI-6130, a potent NS5B inhibitor (**Fig. 5c**), in part owing to an increase in its EC_{50} from 3.49 μM (95% confidence interval (CI) 2.48–4.89) to 6.22 μM (4.43–8.72) and 8.46 μM (7.60–9.44), respectively (**Fig. 5d**). SKI and vitamin E also increased the EC_{50} of MK-7009, an inhibitor of the NS3-4A protease, from 0.488 nM (95% CI 0.411–0.578) to 1.45 nM (1.23–1.72) and 1.90 nM (1.64–2.22), respectively (**Fig. 5e**). The EC_{50} values of other inhibitors targeting NS3-4A (boceprevir) and NS5B (HCV-796 and MK-0608) were similarly increased against H77S.3/GLuc by SKI and vitamin E, but neither SKI nor vitamin E significantly altered the EC_{50} of SCY-635, cyclosporine A, compound 23 or a locked nucleic acid–modified oligonucleotide complementary to miR-122 (anti–miR-122), inhibitors targeting essential HCV host factors, or interferon-α (**Fig. 5f,g** and **Supplementary Fig. 9d–g**). In contrast, SKI and vitamin E caused no change in the EC_{50} of any antiviral against HJ3-5/GLuc (**Fig. 5d,g** and **Supplementary Fig. 9a–f**), indicating that vitamin E and SKI do not impair cellular uptake or metabolism of DAAs. These changes in the EC_{50} against H77S.3/GLuc thus probably reflect altered affinity of the DAAs for NS3-4A and NS5B, suggesting that peroxidation modulates the conformation of these replicase proteins.

Resistance to lipid peroxidation maps to NS4A and NS5B

TNcc is a recently described genotype 1a virus with eight cell culture–adaptive mutations that replicates almost as well as JFH1 in Huh-7.5 cells[34]. Notably, we found it completely resistant to lipid peroxidation (**Fig. 6a** and **Supplementary Fig. 10a**). We introduced all eight TNcc mutations into H77S.3 to determine whether they would confer peroxidation resistance. This RNA (H77S.3/$GLuc_{8mt}$) failed to replicate, but removal of a key H77S.3 adaptive mutation (S2204I in NS5A)[12] restored low-level replication. The resulting virus, H77S.3/$GLuc_{IS/8mt}$, was resistant to lipid peroxidation (**Fig. 6a** and **Supplementary Fig. 10b**). Continued passage of cells infected with $H77S.3_{IS/8mt}$ resulted in the emergence of viruses carrying additional mutations in NS4B (G1909S), NS5A (D2416G) and NS5B (G2963D) that together enhanced replication by 850-fold (**Supplementary Results** and **Supplementary Fig. 11**). The NS4B G1909S mutation

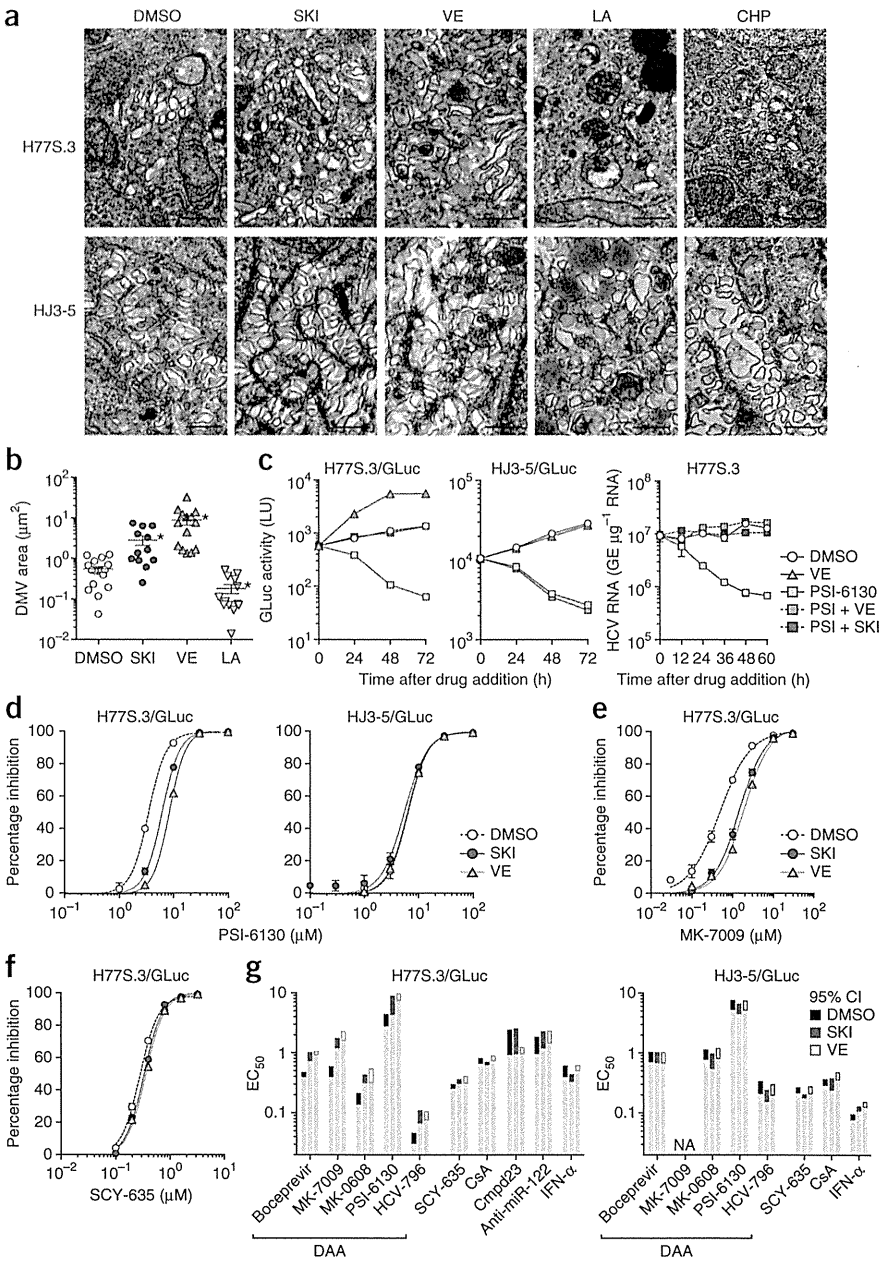

Figure 5 Lipid peroxidation reduces HCV-induced membranous web abundance and alters the EC_{50} of DAAs. (**a**) Transmission electron microscopic images of the membranous web in Huh-7.5 cells electroporated with H77S.3 or HJ3-5 RNA and treated with DMSO, SKI (1 μM), vitamin E (1 μM), linoleic acid (50 μM) or CHP (10 μM). Images shown are representative of 10 different microscopic fields. Scale bars, 500 nm. (**b**) Quantitation of area occupied by double-membrane vesicles (DMV) within individual cells infected with H77S.3 virus and treated with SKI, vitamin E or linoleic acid as in **a**. $*P \leq 0.002$ versus DMSO by two-sided Mann-Whitney *U* test. (**c**) The effect of SKI and vitamin E on the antiviral effect of PSI-6130 against H77S.3/GLuc replication. Left and middle, GLuc produced from Huh-7.5 cells transfected with H77S.3/GLuc or HJ3-5/GLuc RNA 7 d prior to treatment with DMSO, 10 μM PSI-6130, 1 μM vitamin E or both PSI-6130 and either SKI or vitamin E. Right, Cell-associated HCV RNA in similarly treated cells transfected with H77S.3 RNA. Results represent mean ± s.e.m. from two (left, middle) or three (right) replicate cultures. (**d**) Inhibition of H77S.3 (left) and HJ3-5 (right) replication by the NS5B inhibitor PSI-6130 in the presence of SKI or vitamin E (each 1 μM) or DMSO vehicle, assessed by quantifying GLuc secreted 48–72 h after drug addition. Results represent mean ± s.e.m. of two replicate cultures. (**e**,**f**) Inhibition of H77S.3 replication by MK-7009, an NS3-4A inhibitor, (**e**) and SCY-635, a host-targeting cyclophilin inhibitor (**f**). Results represent mean ± s.e.m. of triplicate cultures. (**g**) EC_{50} values of direct-acting versus indirect-acting antivirals against H77S.3 (left) and HJ3-5 (right) viruses in the presence of SKI or vitamin E (each 1 μM). Assays were carried out as in **d**–**f**. Colored bars represent limits of the 95% CI of EC_{50} values calculated from Hill plots. NA, not measureable owing to poor antiviral activity; IFN-α, interferon-α; CsA, cyclosporine A; Cmpd23, compound 23. Additional details are shown in **Supplementary Figure 9**.

compensated for the negative effects on replication of TNcc mutations placed into the H77S.3 background (**Fig. 6b**). When we introduced all three additional mutations (G1909S, D2416G and G2963D) into H77S.3/$GLuc_{IS/8mt}$, the resulting virus (designated H77D) produced infectious virus yields comparable to those of HJ3-5 or JFH1-QL, which were not increased by vitamin E supplementation (**Fig. 6b**). Notably, the EC_{50} of DAAs against H77D virus was not altered by SKI or vitamin E (**Fig. 6d** and **Supplementary Fig. 9h**).

Introducing the G1909S mutation into H77S.3/$GLuc_{IS}$ (H77S.3/$GLuc_{IS/GS}$) did not confer peroxidation resistance (**Fig. 6a**). However, its compensatory effect on the TNcc-derived mutations allowed us to identify the A1672S mutation (in NS4A) from TNcc as essential for peroxidation resistance and to show that TNcc-derived mutations in NS3 and NS4B were not required for this phenotype (**Fig. 6a**). TNcc mutations in NS5B (D2979G, Y2981F and F2994S) were essential for replication of peroxidation-resistant virus, but neither these nor A1672S (in NS4A) alone conferred peroxidation resistance (**Supplementary Fig. 10c**). Thus, mutations in both NS4A and NS5B are required for genotype 1a peroxidation resistance. These mutations are within or in close proximity to the transmembrane domains of these proteins (**Fig. 6c**), consistent with direct involvement of these residues in resistance to lipid peroxidation.

Regulation by lipid peroxidation is unique to HCV

In addition to replication of genotypes 1a (H77S.3) and 1b (HCV-N.2) (**Figs. 2c** and **3a**), replication of HCV genotypes 2a (JFH-2), 3a (S52) and 4a (ED43) was enhanced by treatment with SKI or vitamin E and inhibited by CHP-induced lipid peroxidation (**Fig. 6e**). JFH1 is thus unique among wild-type HCV strains in its resistance to lipid peroxidation.

As with HCV, the genomes of other positive-strand RNA viruses are synthesized by replicase complexes that assemble in association with cytoplasmic membranes and are thus at risk for damage due to lipid peroxidation. Yet, like replication of JFH1, the replication of other

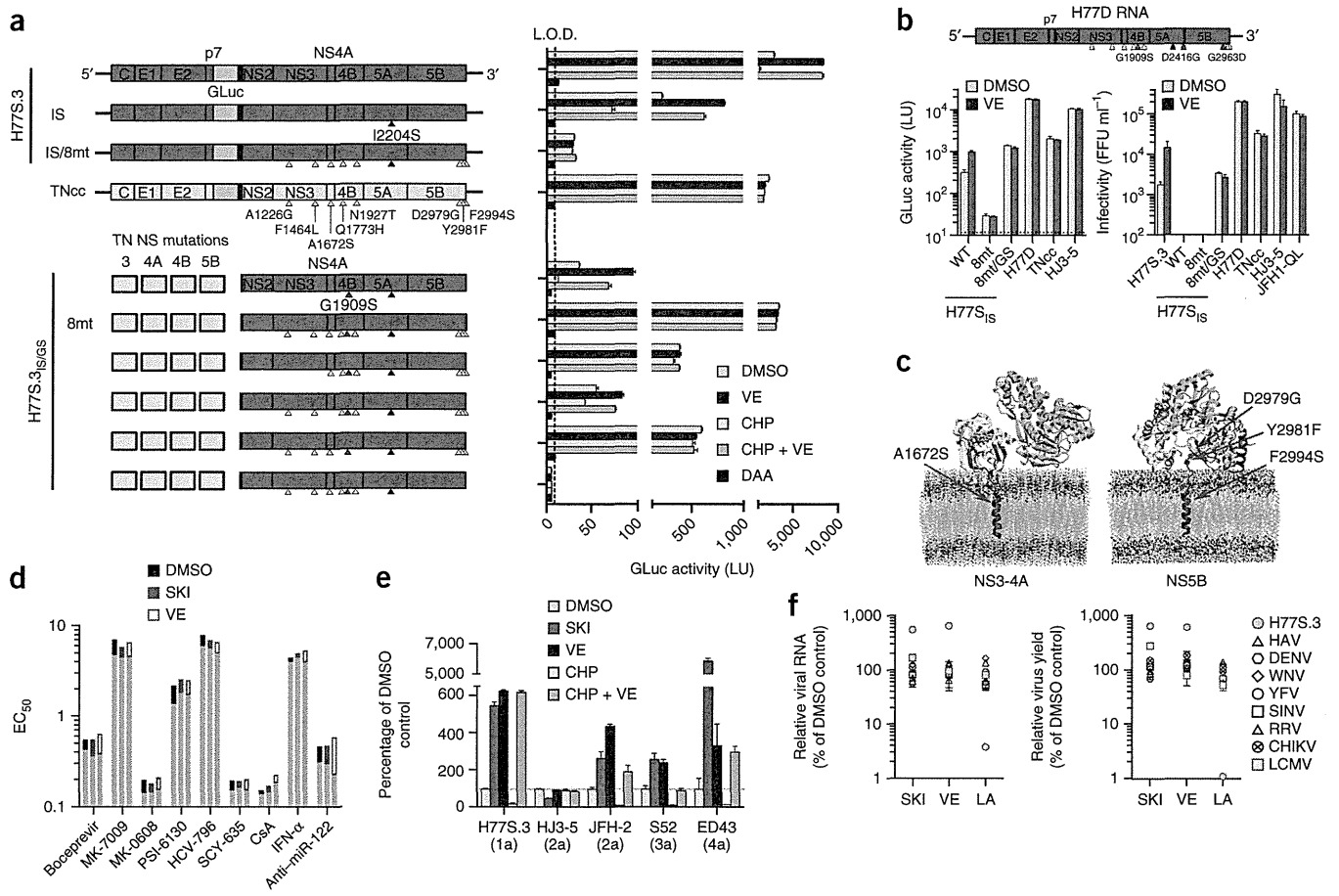

Figure 6 Resistance to lipid peroxidation is tightly linked to robust replication in cell culture. (**a**) Top, cell culture–adaptive mutations in TNcc[34] (yellow arrowheads) that confer resistance to lipid peroxidation when introduced into H77S.3/GLuc$_{IS}$ (H77S.3/GLuc, in which the adaptive mutation S2204I has been removed (black arrowheads); details are shown in **Supplementary Fig. 10b**). GLuc produced from Huh-7.5 cells transfected with indicated RNAs and treated with DMSO, 1 μM SKI, 1 μM vitamin E, 10 μM CHP, CHP plus vitamin E or 30 μM sofosbuvir (DAA). GLuc secreted between 48–72 h is shown. Bottom, role played by TNcc mutations in NS3 (helicase) and NS4B in resistance to lipid peroxidation. Combinations of TNcc substitutions were introduced into H77S.3/GLuc$_{IS/GS}$ (NS proteins shown only) that contains the compensatory mutation G1909S (GS) in NS4B (red arrowhead, **Supplementary Fig. 11**). Data represent mean GLuc activity ± s.e.m. from two independent experiments. (**b**) Top, H77D genome containing the I2204S substitution (black arrowhead), eight TNcc-derived mutations (yellow arrowheads) and three additional compensatory mutations (red arrowheads) in the H77S.3 background. Bottom, GLuc (left) and infectious virus (right) released from Huh-7.5 cells transfected with the indicated RNAs encoding GLuc (left) or lacking GLuc (right) and treated with DMSO or 1 μM vitamin E. Data represent means ± s.d. from triplicate cultures harvested between 48–72 h in a representative experiment. WT, wild-type. (**c**) Structural models of NS4A (left) and NS5B (right) membrane interactions showing key residues that determine sensitivity to lipid peroxidation. (**d**) EC_{50} of direct-acting versus indirect-acting antivirals against H77D in the presence of SKI or vitamin E (each 1 μM). Assays were carried out as in **Figure 5g**. (**e**) Huh-7.5 cells transfected with H77S.3/GLuc or HJ3-5/GLuc RNA, genome-length JFH-2 RNA or subgenomic RNAs (S52 and ED43) encoding firefly luciferase (FLuc) and treated with DMSO, 1 μM SKI or vitamin E, 10 μM CHP or CHP plus vitamin E. Data represent percentage GLuc (H77S.3 and HJ3-5), RNA copies (JFH-2) or FLuc activities (S52 and ED43) at 72 h relative to DMSO controls. Data represent mean ± s.e.m. from three independent experiments. (**f**) The impact of SKI or vitamin E (each 1 μM) or linoleic acid (50 μM) on the abundance of viral RNA (left) or yields of infectious virus (right), as determined for a panel of RNA viruses following infection of Huh-7.5 cells. Data are mean ± s.e.m. from three replicate cultures. Additional details are shown in **Supplementary Figure 12**. HAV, hepatitis A virus; DENV, dengue virus; WNV, West Nile virus; YFV, yellow fever virus; SINV, Sindbis virus; RRV, Ross River virus; CHIKV, Chikungunya virus; LCMV, lymphocytic choriomeningitis virus.

pathogenic positive-strand RNA viruses, including flaviviruses, picornaviruses and alphaviruses, is neither enhanced by SKI or vitamin E nor suppressed by linoleic acid (**Fig. 6f** and **Supplementary Fig. 12a–c**). This is also true for clone 13 lymphocytic choriomeningitis virus, an ambisense RNA virus that establishes persistent infections (**Fig. 6f** and **Supplementary Fig. 12d**). Thus, most viral RNA replicases have evolved in ways that prevent or mitigate the potentially negative effects of lipid peroxidation. HCV is a clear exception, suggesting that its sensitivity to lipid peroxidation may provide a distinct survival advantage.

DISCUSSION

Lipid peroxides are formed on polyunsaturated fatty acid chains within membranes by reactive intermediates produced during oxidative stress. They alter membrane fluidity and permeability and potentially contribute to a variety of disease states[35]. The degradation products of these lipid peroxides include reactive aldehydes, such as acrolein, 4-hydroxy-2-nonenal and MDA, that add to this damage by forming adducts with membrane proteins, thereby modulating their biological activities[35,36]. To our knowledge, the opposing effects of SPHK1 and SPHK2 on lipid peroxidation that we observed

have not been noted previously; they remain unexplained. SPHK1 is predominantly cytosolic and translocates to the plasma membrane upon activation[37], whereas SPHK2 is more likely to be associated with intracellular membranes[28]. Sphingosine-1-phosphate produced by SPHK functions as a messenger in several signaling pathways and is a cofactor for enzymes involved in signal transduction and transcriptional regulation[38,39]. However, it has no effect on HCV replication in cell cultures and only minimally increases MDA abundance (**Supplementary Fig. 1c,d**).

During HCV infection, oxidative stress is caused by both host inflammatory responses and direct interactions of viral proteins with mitochondria[7,40]. Our results show that the wild-type H77c and N replicases are highly sensitive to both endogenous and PUFA-induced lipid peroxidation. Con1 and OR6, two other genotype 1 HCVs, are also inhibited by PUFA-induced peroxidation[8,41]. Given that we found that lipid peroxidation also inhibits multiple other HCV genotypes, we conclude that this sensitivity to peroxidation is a common feature of HCV.

In genotype 1a H77S.3 virus, we found that resistance to lipid peroxidation maps to residues within or near the transmembrane domains of NS4A and NS5B, key components of the replicase complex. Reactive aldehydes derived from degraded lipid peroxides could form adducts with residues within these transmembrane domains, impairing their capacity for essential interactions and thereby reducing replicase activity. The A1672S mutation promotes oligodimerization of the NS4A transmembrane domain, an interaction necessary for efficient replicase function[42]. Thus, A1672S might confer resistance to peroxidation by restoring NS4A dimerization impaired by adduct formation. Adduct formation could similarly affect the NS5B transmembrane domain. Although hypothetical, such effects could explain the changes we observed in the EC_{50} of DAAs targeting NS3-4A and NS5B. Alternatively, proper membrane localization and assembly of nonstructural proteins within the replicase may require lipids esterified with nonoxidized fatty acid chains. Indeed, we found that monounsaturated fatty acid supplements such as oleic acid stimulate H77S.3/GLuc and N.2/GLuc replication but not that of JFH1 (**Supplementary Fig. 5h**). A third possibility is that lipid peroxidation could induce changes in membrane fluidity that alter replicase conformation[35].

We propose that HCV exploits lipid peroxidation as a means of autoregulating its replication and that lipid peroxides act as a brake, downregulating the efficiency of genome amplification when reaching a threshold abundance (**Supplementary Fig. 13**). Such a model suggests that HCV possesses a conserved peroxidation 'sensor', mapping in part to the transmembrane domains of NS4A and NS5B, that governs replication efficiency, thereby limiting tissue damage, reducing viral exposure to the immune system and facilitating viral persistence. Although hepatotoxicity associated with diets deficient in lipophilic antioxidants presents a technical barrier to testing this hypothesis in murine models of HCV[43], our results show that in primary human hepatocytes, HCV replication is regulated by lipid peroxidation. Related RNA viruses that are capable of establishing persistent infection appear to autorestrict replication via alternative mechanisms. For example, bovine viral diarrhea virus, a pestivirus that establishes lifelong persistence, downregulates replicase formation by limiting cleavage of its NS2-3 protein, thereby arresting RNA synthesis and enabling a noncytolytic phenotype[44]. Thus, reducing the efficiency of the replicase may be a common theme for RNA viruses that establish persistent infection.

Like most other positive-strand RNA viruses, the genotype 2a JFH1 virus is highly resistant to lipid peroxidation. This suggests that JFH1 may be a loss-of-function mutant that no longer senses lipid peroxides and autorestricts its replicase activity. Whether the original JFH1 patient isolate similarly lacked the ability to be regulated by lipid peroxidation is uncertain, as is the possibility that lack of peroxidation sensitivity contributed in some way to the fulminant hepatitis experienced by this patient[9]. Only one of the four amino acid substitutions conferring peroxidation resistance in H77S.3 (NS5B F2981) exists in JFH1, and the molecular basis of its peroxidation resistance remains to be determined. Nonetheless, our results provide a basis for understanding the robust capacity of the JFH1 virus to replicate in cell culture. Our findings also highlight the uniqueness of HCV regulation by lipid peroxidation among other pathogenic RNA viruses and its potential importance to the pathogenesis of chronic hepatitis C.

METHODS

Methods and any associated references are available in the online version of the paper.

Note: Any Supplementary Information and Source Data files are available in the online version of the paper.

ACKNOWLEDGMENTS

We thank L.F. Ping and W. Lovell for expert technical assistance, R. Purcell (US National Institute of Allergy and Infectious Diseases) and J. Bukh (Copenhagen University Hospital, Denmark) for pCV-H77C and pTNcc plasmids, C.M. Rice and M. Saeed (The Rockefeller University) for Huh-7.5 cells and S52/SG-Feo and ED43/SG-Feo plasmids, T. Wakita (National Institute of Infectious Diseases, Japan) for pJFH1 and pJFH-2 plasmids, M.J. Otto (Pharmasset) for PSI-6130, A. Sluder (SCYNEXIS) for SCY-635, R. De Francesco (Istituto Nazionale di Genetica Molecolare, Italy) for compound 23, A.Y. Howe (Merck Research Laboratory) for boceprevir, HCV-796, MK-0608 and MK-7009 and Z. Feng (University of North Carolina) for hepatitis A virus stocks. We also thank S.A. Weinman for critical reading of the manuscript and D.L. Tyrrell, M. Joyce, R.A. Coleman and T. Masaki for helpful discussions. This work was supported by US National Institutes of Health grants RO1-AI095690, RO1-CA164029 and U19-AI109965 (S.M.L.), R21-CA182322 (L.R.), R01-AI075090 (M.Y.), RO1-AI073335 (C.C.K.), RO1-DE018304 (D.P.D.), F32-AI094941 (D.G.W.) and U54-GM069338 (S.B.), a National Cancer Institute Center Core Support Grant to the Lineberger Comprehensive Cancer Center (P30-CA016086) and the University of North Carolina Cancer Research Fund. C.W. was supported by the Deutsche Forschungsgemeinschaft (WE 4388/3-1 and WE 4388/6-1). I.A. was supported by the CIPSM Cluster of Excellence.

AUTHOR CONTRIBUTIONS

D.Y. and S.M.L. conceived the study and wrote the paper; D.Y., D.R.M., E.W., V.J.M., Y.W., P.E.C., C.E.M., D.G.W. and I.M. conducted experiments; C.W. and I.A. modeled membrane interactions of proteins; S.B. and A.H.M. Jr. carried out mass spectrometry analysis of sphingolipids; J.K.W., M.T.H., D.P.D. and C.C.K. provided reagents and supervised experiments involving viruses other than HCV; M.Y., S.K., T.S., T.O., S.M.P. and L.M.R. provided research materials; and all authors discussed the results and commented on the manuscript.

COMPETING FINANCIAL INTERESTS

The authors declare competing financial interests: details are available in the online version of the paper.

1. Kalyanaraman, B. Teaching the basics of redox biology to medical and graduate students: oxidants, antioxidants and disease mechanisms. *Redox. Biol.* **1**, 244–257 (2013).
2. Nathan, C. & Cunningham-Bussel, A. Beyond oxidative stress: an immunologist's guide to reactive oxygen species. *Nat. Rev. Immunol.* **13**, 349–361 (2013).
3. Dennery, P.A. Effects of oxidative stress on embryonic development. *Birth Defects Res. C Embryo Today* **81**, 155–162 (2007).
4. Valyi-Nagy, T. & Dermody, T.S. Role of oxidative damage in the pathogenesis of viral infections of the nervous system. *Histol. Histopathol.* **20**, 957–967 (2005).
5. Thomas, D.L. Global control of hepatitis C: where challenge meets opportunity. *Nat. Med.* **19**, 850–858 (2013).
6. Choi, J. Oxidative stress, endogenous antioxidants, alcohol, and hepatitis C: pathogenic interactions and therapeutic considerations. *Free Radic. Biol. Med.* **52**, 1135–1150 (2012).

7. Okuda, M. *et al.* Mitochondrial injury, oxidative stress, and antioxidant gene expression are induced by hepatitis C virus core protein. *Gastroenterology* **122**, 366–375 (2002).
8. Huang, H., Chen, Y. & Ye, J. Inhibition of hepatitis C virus replication by peroxidation of arachidonate and restoration by vitamin E. *Proc. Natl. Acad. Sci. USA* **104**, 18666–18670 (2007).
9. Wakita, T. *et al.* Production of infectious hepatitis C virus in tissue culture from a cloned viral genome. *Nat. Med.* **11**, 791–796 (2005).
10. Lindenbach, B.D. *et al.* Complete replication of hepatitis C virus in cell culture. *Science* **309**, 623–626 (2005).
11. Zhong, J. *et al.* Robust hepatitis C virus infection *in vitro*. *Proc. Natl. Acad. Sci. USA* **102**, 9294–9299 (2005).
12. Yi, M., Villanueva, R.A., Thomas, D.L., Wakita, T. & Lemon, S.M. Production of infectious genotype 1a hepatitis C virus (Hutchinson strain) in cultured human hepatoma cells. *Proc. Natl. Acad. Sci. USA* **103**, 2310–2315 (2006).
13. Pietschmann, T. *et al.* Production of infectious genotype 1b virus particles in cell culture and impairment by replication enhancing mutations. *PLoS Pathog.* **5**, e1000475 (2009).
14. Paul, D., Hoppe, S., Saher, G., Krijnse-Locker, J. & Bartenschlager, R. Morphological and biochemical characterization of the membranous hepatitis C virus replication compartment. *J. Virol.* **87**, 10612–10627 (2013).
15. Gosert, R. *et al.* Identification of the hepatitis C virus RNA replication complex in Huh-7 cells harboring subgenomic replicons. *J. Virol.* **77**, 5487–5492 (2003).
16. Shi, S.T., Lee, K.J., Aizaki, H., Hwang, S.B. & Lai, M.M. Hepatitis C virus RNA replication occurs on a detergent-resistant membrane that cofractionates with caveolin-2. *J. Virol.* **77**, 4160–4168 (2003).
17. Hsu, N.Y. *et al.* Viral reorganization of the secretory pathway generates distinct organelles for RNA replication. *Cell* **141**, 799–811 (2010).
18. Reiss, S. *et al.* Recruitment and activation of a lipid kinase by hepatitis C virus NS5A is essential for integrity of the membranous replication compartment. *Cell Host Microbe* **9**, 32–45 (2011).
19. Saxena, V., Lai, C.K., Chao, T.C., Jeng, K.S. & Lai, M.M. Annexin A2 is involved in the formation of hepatitis C virus replication complex on the lipid raft. *J. Virol.* **86**, 4139–4150 (2012).
20. Romero-Brey, I. *et al.* Three-dimensional architecture and biogenesis of membrane structures associated with hepatitis C virus replication. *PLoS Pathog.* **8**, e1003056 (2012).
21. Miyanari, Y. *et al.* The lipid droplet is an important organelle for hepatitis C virus production. *Nat. Cell Biol.* **9**, 1089–1097 (2007).
22. Aizaki, H. *et al.* Critical role of virion-associated cholesterol and sphingolipid in hepatitis C virus infection. *J. Virol.* **82**, 5715–5724 (2008).
23. Sakamoto, H. *et al.* Host sphingolipid biosynthesis as a target for hepatitis C virus therapy. *Nat. Chem. Biol.* **1**, 333–337 (2005).
24. Umehara, T. *et al.* Serine palmitoyltransferase inhibitor suppresses HCV replication in a mouse model. *Biochem. Biophys. Res. Commun.* **346**, 67–73 (2006).
25. Hirata, Y. *et al.* Self-enhancement of hepatitis C virus replication by promotion of specific sphingolipid biosynthesis. *PLoS Pathog.* **8**, e1002860 (2012).
26. Weng, L. *et al.* Sphingomyelin activates hepatitis C virus RNA polymerase in a genotype-specific manner. *J. Virol.* **84**, 11761–11770 (2010).
27. Shimakami, T. *et al.* Protease inhibitor-resistant hepatitis C virus mutants with reduced fitness from impaired production of infectious virus. *Gastroenterology* **140**, 667–675 (2011).
28. Liu, H. *et al.* Molecular cloning and functional characterization of a novel mammalian sphingosine kinase type 2 isoform. *J. Biol. Chem.* **275**, 19513–19520 (2000).
29. Kapadia, S.B. & Chisari, F.V. Hepatitis C virus RNA replication is regulated by host geranylgeranylation and fatty acids. *Proc. Natl. Acad. Sci. USA* **102**, 2561–2566 (2005).
30. Lindenbach, B.D. *et al.* Cell culture-grown hepatitis C virus is infectious *in vivo* and can be recultured *in vitro*. *Proc. Natl. Acad. Sci. USA* **103**, 3805–3809 (2006).
31. Yanagi, M., Purcell, R.H., Emerson, S.U. & Bukh, J. Transcripts from a single full-length cDNA clone of hepatitis C virus are infectious when directly transfected into liver of a chimpanzee. *Proc. Natl. Acad. Sci. USA* **94**, 8738–8743 (1997).
32. Beard, M.R. *et al.* An infectious molecular clone of a Japanese genotype 1b hepatitis C virus. *Hepatology* **30**, 316–324 (1999).
33. Andrus, L. *et al.* Expression of paramyxovirus V proteins promotes replication and spread of hepatitis C virus in cultures of primary human fetal liver cells. *Hepatology* **54**, 1901–1912 (2011).
34. Li, Y.P. *et al.* Highly efficient full-length hepatitis C virus genotype 1 (strain TN) infectious culture system. *Proc. Natl. Acad. Sci. USA* **109**, 19757–19762 (2012).
35. Bochkov, V.N. *et al.* Generation and biological activities of oxidized phospholipids. *Antioxid. Redox Signal.* **12**, 1009–1059 (2010).
36. Pizzimenti, S. *et al.* Interaction of aldehydes derived from lipid peroxidation and membrane proteins. *Front. Physiol.* **4**, 242 (2013).
37. Pitson, S.M. *et al.* Activation of sphingosine kinase 1 by ERK1/2-mediated phosphorylation. *EMBO J.* **22**, 5491–5500 (2003).
38. Alvarez, S.E. *et al.* Sphingosine-1-phosphate is a missing cofactor for the E3 ubiquitin ligase TRAF2. *Nature* **465**, 1084–1088 (2010).
39. Hait, N.C. *et al.* Regulation of histone acetylation in the nucleus by sphingosine-1-phosphate. *Science* **325**, 1254–1257 (2009).
40. Jain, S.K. *et al.* Oxidative stress in chronic hepatitis C: not just a feature of late stage disease. *J. Hepatol.* **36**, 805–811 (2002).
41. Yano, M. *et al.* Comprehensive analysis of the effects of ordinary nutrients on hepatitis C virus RNA replication in cell culture. *Antimicrob. Agents Chemother.* **51**, 2016–2027 (2007).
42. Kohlway, A. *et al.* Hepatitis C virus RNA replication and virus particle assembly require specific dimerization of the NS4A protein transmembrane domain. *J. Virol.* **88**, 628–642 (2014).
43. Ibrahim, W. *et al.* Oxidative stress and antioxidant status in mouse liver: effects of dietary lipid, vitamin E and iron. *J. Nutr.* **127**, 1401–1406 (1997).
44. Lackner, T., Muller, A., Konig, M., Thiel, H.J. & Tautz, N. Persistence of bovine viral diarrhea virus is determined by a cellular cofactor of a viral autoprotease. *J. Virol.* **79**, 9746–9755 (2005).

ONLINE METHODS

Cells and reagents. Huh-7.5 cells were grown in Dulbecco's modified Eagle's medium (DMEM), High Glucose supplemented with 10% fetal bovine serum (FBS), 1× penicillin-streptomycin, 1× GlutaMAX and 1× MEM Non-Essential Amino Acids Solution (Gibco). BD-BioCoat collagen-I coated plates were purchased from BD Biosciences. SKI (2-(*p*-hydroxyanilino)-4-(*p*-chlorophenyl) thiazole) was obtained from Merck Millipore. Myriocin, fumonisin B1, *N*-[2-hydroxy-1-(4-morpholinylmethyl)-2-phenylethyl]-decanamide (PDMP), D-erythro-2-tetradecanoylamino-1-phenyl-1-propanol (D-MAPP), dihydrosphingosine, C-2 and C-8 ceramides, sphingosine, sphingosine 1-phosphate, lovastatin, ebselen, arachidonic acid, docosahexaenoic acid and linoleic acid were from Cayman Chemical. Vitamin E (α-, *rac*-β- and γ-tocopherols), 4-deoxypyridoxine hydrochloride (DOP), coenzyme Q10, butylated hydroxytoluene, *N*-acetyl-L-cysteine, diphenyleneiodonium chloride, oleic acid and cyclosporine A were from Sigma-Aldrich. nSMase spiroepoxide and cumene hydroperoxide were from Santa Cruz Biotechnology; D609 was from Enzo Life Sciences; and sofosbuvir (PSI-7977) was from Chemscene. Locked nucleic acid anti-miR-122 was synthesized by Exiqon. A selective PI4KIIIα inhibitor, compound 23 (ref. 45), was provided by R. De Francesco. Relative cell numbers were assessed using the WST-1 reagent (Millipore) or determination of protein content. Protein concentrations in samples were determined using the Protein Assay kit (Bio-Rad) with bovine serum albumin as a standard.

Fetal liver cells. Tissue samples were supplied by the accredited nonprofit corporation Advanced Biosciences Resources, Inc. (ABR) and obtained from fetuses between 15–20 weeks gestation during elective terminations of pregnancy. Tissues were collected with written informed consent from all donors and in accordance with the US Food and Drug Administration CFR Part 1271 Good Tissue Practices regulations. Tissue was processed as described elsewhere[46–48], and isolated hepatoblasts were seeded at density of 5.2×10^5 cm^{-2} on 12- or 24-well plates and in regular Kubota's Medium[49] supplemented with 5% FBS. Following an overnight incubation, the medium was changed to a variation of Kubota's Medium (HFH medium) comprised of DMEM supplemented with 25 mM HEPES, 1 nM selenium, 0.1% BSA, 4.5 mM niacinamide, 0.1 nM zinc sulfate heptahydrate, 10 nM hydrocortisone, 5 μg ml^{-1} transferrin/Fe, 5 μg ml^{-1} insulin, 2 mM L-glutamine, antibiotics and 2% FBS. The use of commercially procured fetal liver cells was reviewed by the University of North Carolina at Chapel Hill Office of Human Research Ethics and was determined not to require approval by the University of North Carolina at Chapel Hill Institutional Review Board.

Plasmids. pHJ3-5 (ref. 50), pHJ3-5/GLuc2A (referred to here as pHJ3-5/GLuc), pHJ3-5/GND, pH77c (ref. 51), pH77S.3, pH77S.3/GLuc2A (referred to here as pH77S.3/GLuc) and pH77S/GLuc2A-AAG (refs. 12,27,52) have been described. pHCV-N.2 is a modified version of HCV3-9b (ref. 32) that contains cell culture–adaptive mutations in NS3 and NS5A (A1099T, E1203G and S2204I in the polyprotein). Mutations in the sphingomyelin binding domain, 5′ UTR, 3′ UTR and nonstructural protein regions were generated by site-directed mutagenesis. The *Gaussia princeps* luciferase (GLuc)-coding sequence followed by the foot-and-mouth disease virus 2A protease–coding sequence was inserted between p7 and NS2 in pH77c, pHCV-N.2, pJFH1 (wild-type) and pJFH1-QL (containing the cell culture–adaptive mutation Q221L in the NS3 helicase) using a strategy applied previously to pH77S (ref. 27). JFH1-QL was used for experiments unless otherwise indicated. Other cell culture–adapted genotype 1a (TNcc), 2a (JFH-2/AS/mtT3), 3a (S52/SG-Feo(SH)) and 4a (ED43/SG-Feo(K)) HCV strains and RNA replicons have been described[34,53,54].

Luciferase assays. For the *Gaussia* luciferase (GLuc) assay, cells transfected with HCV RNA encoding GLuc were treated with drugs at 6 h after transfection, and the culture medium was harvested, refed with fresh medium containing drugs and assayed for GLuc at 24-h intervals. Secreted GLuc activity was measured as described[52]. For the firefly luciferase (FLuc) assay, cell monolayers were washed with PBS and lysed in Passive Lysis Buffer (Promega), and the lysates were analyzed with the Luciferase Assay System (Promega) according to the manufacturer's instructions. For each individual experiment, we used duplicate or triplicate cell cultures. Results shown represent the mean ± s.e.m. from multiple independent experiments.

RNA transcription. RNA transcripts were synthesized *in vitro* as described previously[27].

Hepatitis C virus RNA transfection. At 24 h before transfection, 7.5×10^4 Huh-7.5 cells were seeded onto a 24-well plate. One day later, medium was replaced with fresh medium, and the cells were transfected with 0.25 μg (per well) HCV RNA–encoding GLuc using the TransIT mRNA transfection kit (Mirus) according to the manufacturer's protocol. After 6 h incubation at 37 °C, supernatant fluids were removed for GLuc assay and replaced with fresh medium-containing compound. Alternatively, 10 μg of HCV RNA was mixed with 5×10^6 Huh-7.5 cells and electroporated into cells using a Gene Pulser Xcell Total System (Bio-Rad) as described previously[52]. Transfection of wild-type HCV RNA was performed by electroporating 5 μg HCV RNA in 2.5×10^6 Huh-7.5 cells and seeded into collagen-coated plates (BD Biosciences). Cells were grown in DMEM supplemented with 25 mM HEPES, 7 ng ml^{-1} glucagon, 100 nM hydrocortisone, 5 μg ml^{-1} insulin, 2 mM GlutaMAX, antibiotics and 2% FBS. Culture supernatants were replaced with the medium supplemented with drugs at 6 h and every 48 h thereafter and assayed for GLuc activity.

Hepatitis C virus production. For virus production, subconfluent Huh-7.5 cells in a 100-mm diameter dish were transfected with 5 μg HCV RNA using the TransIT mRNA transfection kit as above and split at 1:2 ratio at 6 h after transfection. Cells were then fed with medium supplemented with 50 mM HEPES (Cellgro) and the supernatants harvested and replaced with fresh medium every 24 h. Cells were passaged at a 1:2 ratio again 3 d after transfection. Medium containing HCV was supplemented with an additional 50 mM HEPES and stored at 4 °C until assayed for infectivity. *Gaussia* luciferase H77S.3/GLuc reporter virus was produced by electroporating 5 μg H77S.3/GLuc RNA into 2.5×10^6 Huh-7.5 cells. Cells were fed with medium containing 25 mM HEPES and 10 μM vitamin E at 3 h and grown for 3 d until subconfluent. Cells were then split 1:3 into medium containing 25 mM HEPES. Supernatant fluids, harvested on the following day, were stored at 4 °C until use. HJ3-5/GLuc virus was produced in medium lacking vitamin E and stored in −80 °C until use. Infectious titers were determined by $TCID_{50}$ using GLuc activity produced at 72 h after inoculation.

Hepatitis C virus infectivity assays. Huh-7.5 cells were seeded at 5×10^4 cells per well into 48-well plates 24 h before inoculation with 100 μl of culture medium. Cells were fed with medium containing 1 μM vitamin E 24 h later to facilitate visualization of core protein expression, fixed with methanol-acetone (1:1) at −20 °C for 10 min 72 h after inoculation (48 h for JFH1-QL and HJ3-5) and stained for intracellular core antigen with a mouse monoclonal antibody C7–50 (Thermo Scientific, 1:300 dilution). Clusters of infected cells identified by staining for core antigen were considered to constitute a single infectious focus, and the data were expressed as focus-forming units (FFU) ml^{-1}.

Hepatitis C virus infection in fetal hepatoblasts. Cells were inoculated with HCV encoding GLuc (MOI = 0.001) for 6 h. After washing five times with HFH medium, cells were incubated for an additional 18 h to determine baseline GLuc secretion. Culture supernatant fluids were replaced at 24 h intervals with HFH medium containing drugs and assayed for GLuc.

Flow cytometry. Huh-7.5 cells electroporated with H77S.3 or HJ3-5 RNA were treated with 1 μM SKI or DMSO beginning at 24 h and analyzed for NS5A expression by flow cytometry at 96 h. Virus spread assays were adapted from a previously described method[55]. Briefly, Huh-7.5 cells were electroporated with H77S.3, HJ3-5 or HJ3-5/GND RNAs and cultured for 24 h. The electroporated (producer) cells were then cocultured at a 1:4 ratio with naive Huh-7.5 (recipient) cells prelabeled with 5 μM carboxyfluorescein diacetate succinimidyl ester (CellTrace CFSE Cell Proliferation Kit, Invitrogen) in the presence of different compounds (see figure legends) for 48 h. Cells were stained for NS5A protein and analyzed by flow cytometry as described previously[56].

Equilibrium ultracentrifugation. Filtered supernatant fluids collected from transfected cell cultures were concentrated 50-fold using Centricon Plus-70 Centrifugal Filter Units (100-kDa exclusion) (Millipore) and then layered on top of a preformed continuous 10–40% iodixanol (OptiPrep, Sigma-Aldrich)

doi:10.1038/nm.3610

gradient in Hank's balanced salt solution (HBSS, Invitrogen). Gradients were centrifuged in a SureSpin 630 Swinging Bucket Rotor (Thermo Scientific) at 30,000 r.p.m. for 24 h at 4 °C, and fractions were collected from the top of the tube. The density of each fraction was calculated from the refractive index measured with a refractometer (ATAGO). RNA was isolated from each fraction using QIAamp Viral RNA kit (Qiagen) and the viral amount quantified by qRT-PCR as described below. Infectious virus titers in each fraction were determined as described above.

qRT-PCR. One-step qRT-PCR analysis of HCV RNA in Huh-7.5 cells was carried out as described[52]. HCV RNA in primary human fetal hepatoblast cultures was detected by means of a two-step qRT-PCR procedure using SuperScript III First-Strand Synthesis SuperMix for qRT-PCR (Invitrogen), followed by TaqMan qPCR analysis with primer pairs and a probe targeting a conserved 221-base sequence within the 5′ UTR of the genome and iQ Supermix (Bio-Rad)[52].

RNA interference. Validated siRNA targeting human *SPHK1* (SI02660455)[57] was purchased from Qiagen. siRNA targeting human *SPHK2* (5′-CGUCAC GGUUAAAGAGAAA-3′)[39] and control siRNA (#2) were from Dharmacon. siRNA (20 nM) was transfected into cells using siLentfect Lipid Reagent (Bio-Rad) according to the manufacturer's protocol.

Immunoblots. Immunoblotting was carried out using standard methods with the following antibodies: mouse monoclonal antibodies to β-actin (AC-74, Sigma, 1:10,000), HCV NS3 (ab65407, Abcam, 1:500) and rabbit polyclonal antibodies to SPHK1 (A302-177A, Bethyl Laboratories, 1:2,000) or SPHK2 (ab37977, Abcam, 1:500). Protein bands were visualized and quantified with an Odyssey Infrared Imaging System (Li-Cor Biosciences).

Sphingosine kinase assay. Sphingosine kinase activity was determined as described previously[28]. Recombinant human SPHK1 and SPHK2 proteins were obtained from BPS Bioscience. SPHK1 activity was determined in the presence of 0.25% Triton X-100, which inhibits SPHK2 (ref. 28). The labeled S1P was separated by TLC on Silica Gel G-60 (Whatman) with 1-butanol/ethanol/acetic acid/water (80:20:10:20, v/v) and visualized and quantified by phosphorimager (Bio-Rad).

Quantification of cholesterol and triglyceride levels. Cells were scraped and lysed in PBS containing 1% Triton X-100 and complete protease inhibitor cocktail (Roche). Cell lysates were clarified by centrifugation at 15,000 r.p.m. at 4 °C for 10 min. Cholesterol contents were determined using the Amplex Red Cholesterol Assay Kit (Invitrogen) according to the manufacturer's protocol. Triglyceride levels in cells grown on 96-well plates were determined using Triglyceride Assay Kit (Zen-Bio) as per manufacturer's instruction. The values were normalized to the total protein content.

Lipid peroxidation assays. Malondialdehyde (MDA), a product of lipid peroxidation, was quantified by the thiobarbituric acid reactive substances (TBARS) Assay Kit (Cayman Chemical). Cells transfected with HCV RNAs were grown in the presence of different drugs and analyzed for intracellular malondialdehyde (MDA) abundance at 48–72 h as indicated in legends. Cells scraped into PBS containing complete protease inhibitor cocktail (Roche) were homogenized by sonication on ice using Sonic Dismembrator (FB-120, Fisher Scientific). The amount of MDA in 100 μl of cell homogenates was analyzed by a fluorescent method as described by the manufacturer. Lipid peroxidation levels were expressed as the amount of MDA normalized to the amount of total protein. Alternatively, the lipid peroxidation product, 8-isoprostane, was quantified using the 8-Isoprostane EIA kit (Cayman Chemical) according to the manufacturer's recommended procedures.

Innate immune response reporter assays. IFN-β–, IRF-3– and NF-κB–dependent promoter activities were assayed using firefly luciferase reporters pIFN-β-Luc, p4xIRF3-Luc or pPRDII-Luc as described previously[58]. Cells were cotransfected with the reporter plasmid pRL-CMV, and the firefly luciferase results were normalized to *Renilla* luciferase activity in order to control for potential differences in transfection efficiency. The luminescence was measured on a Synergy 2 (Bio-Tek) Multi-Mode Microplate Reader.

Mass spectrometry of sphingolipids and metabolites. Cells were washed extensively with PBS and scraped into tubes. An aliquot of cells was taken for protein and total lipid phosphate measurements. After addition of a sphingolipid internal standard cocktail (Avanti Polar Lipids), the lipids were extracted, and individual sphingolipid species were quantified by liquid chromatography, electrospray ionization-tandem mass spectrometry as described previously[59,60].

Electron microscopy. Huh-7.5 cells (5×10^6 cells) electroporated with 5 μg HCV RNA were seeded into a 6-well plate, and medium containing compounds was added 24 h later. At 48 h after transfection, cells were fixed with 3% glutaraldehyde in 0.15 M sodium phosphate buffer, pH 7.4, for 1 h at room temperature and stored at 4 °C until processed. Following three rinses with 0.15 M sodium phosphate buffer, pH 7.4, monolayers were postfixed with 1% osmium tetroxide for 1 h, washed in deionized water and stained *en bloc* with 2% aqueous uranyl acetate for 20 min. The cells were dehydrated using increasing concentrations of ethanol (30%, 50%, 75%, 100%, 100%, 10 min each) and embedded in Polybed 812 epoxy resin (Polysciences, Inc.). Cell layers were sectioned *en face* to the substrate at 70 nm using a diamond knife and a Leica Ultracut UCT microtome (Leica Microsystems). Ultrathin sections were mounted on 200 mesh copper grids and stained with 4% aqueous uranyl acetate and Reynolds' lead citrate[61]. The grids were observed at 80 kV using a LEO EM910 transmission electron microscope (Carl Zeiss SMT, LLC). Digital images were taken using a Gatan Orius SC 1000 CCD Camera with DigitalMicrograph 3.11.0 software (Gatan, Inc.).

Peroxidation resistance of hepatitis A virus, flavivirus, alphavirus and lymphocytic choriomeningitis virus replicases. Virus stocks were provided as follows: HAV by Z. Feng and S.M.L.; YFV and WNV by D.P.D.; DENV by D.G.W.; SINV, RRV and CHIKV by M.T.H.; and LCMV by J.K.W. The abundance of HAV, RRV, SINV and LCMV RNA was determined using iScript One-Step RT-PCR kit with SYBR green (Bio-Rad) and primer pairs as follows: HAV forward 5′-GGTAGGCTACGGGTGAAAC-3′ and reverse 5′-AACAACTCACCAATATCCGC-3′, RRV forward 5′-AGAGT GCGGAAGACCCAGAG-3′ and reverse 5′-CCGTGATCTTACCGGACA CA-3′, SINV forward 5′-GAGGTAGTAGCACAGCAGG-3′, and reverse 5′-CG GAAAACATTCTACGAGC-3′ and LCMV forward 5′-CATTCACCTGGACTTT GTCAGACTC-3′ and reverse 5′-GCAACTGCTGTGTTCCCGAAAC-3′. WNV and YFV RNA levels were quantified using a previously described method[62] with primers as follows: WNV forward 5′-TCAGCGATCTCTCCACCAAAG-3′ and reverse 5′-GGGTCAGCACGTTTGTCATTG-3′ and YFV forward 5′-CT GTCCCAATCTCAGTCC-3′ and reverse 5′-AATGCTCCCTTTCCCAAA TA-3′. DENV RNA was quantified on a 7900 HT Real-Time PCR System (ABI) using primers and probe as described[63].

The infrared fluorescent immunofocus assay for infectious hepatitis A virus (HAV) was done using FRhK-4 cells as previously described[64]. Titration of infectious alphaviruses was performed in duplicate by visualization of plaques on Vero cells seeded in 12-well plates. Plates were incubated with inoculum at 37 °C with 5% CO_2 for 1 h with periodic agitation. Inocula were then removed and plates overlaid with 1.25% carboxymethylcellulose in MEM supplemented with 3% FBS, 1× penicillin-streptomycin, 2 mM L-glutamine and HEPES. All of these reagents were identical to those used for parallel studies of HCV. At 48 h after infection, plates were fixed with 4% paraformaldehyde and visualized with a 0.25% crystal violet solution. Infectious titers of WNV and YFV were determined by plaque assay on confluent BHK cell monolayers in 6-well plates. Cells were incubated with virus inocula for 2 h at 37 °C, washed before addition of a 1% methylcellulose medium overlay and further incubated for 3 d. Plaques were visualized with Giemsa staining. DENV titers were determined by plaque assay on Vero 76 cell monolayers in 96-well plates. Cells were incubated with virus inocula for 2 h at 37 °C, washed before addition of a 0.8% methylcellulose medium overlay and further incubated for 3 d. Following fixation with ice-cold acetone methanol solution (50:50 v/v), cells were immunostained using the DENV E–specific monoclonal antibody 4G2 (UNC Antibody Core Facility, 1:500) followed by HRP-conjugated anti-mouse IgG secondary antibody (KPL, 464-1806, 1:1,000). Infectious foci were visualized using Vector VIP reagent (Vector Labs). LCMV titers were determined by plaque assay on confluent Vero cell monolayers in 6-well plates[65]. Cells were incubated with virus inocula for 80 min at 37 °C before addition of a 1:1 mixture of 1% agarose and EMEM medium containing 10% FCS, 2 mM L-glutamine, 2% penicillin and

2% streptomycin. Cells were further incubated for 5 d at 37 °C. Plaques were visualized with crystal violet.

Modeling of hepatitis C virus nonstructural protein-membrane interactions. Membrane topologies of HCV nonstructural proteins were modeled as suggested by Bartenschlager *et al.*[66] using the Protein Data Bank (PDB) structure 4A92 for the NS3-4A protease-helicase (**Fig. 6c**) and PDB 1GX6 for the NS5B RNA-dependent RNA polymerase (**Fig. 6c**). Secondary structure predictions were generated on the Jpred3 server (http://www.compbio.dundee.ac.uk/www-jpred/). Visual Molecular Dynamics (VMD) with the plugin "Membrane" was applied for visualization of protein-membrane interactions[67].

Statistical analyses. Unless noted otherwise, all between-group comparisons were carried out by two-way ANOVA using Prism 6.0 software (GraphPad Software, Inc.). For determination of EC_{50} concentrations of DAAs, data were fit to a four-parameter dose-response curve with variable slope using Prism 5.0c for Mac OS X software (GraphPad Software, Inc.). Results are reported as the estimated $EC_{50} \pm 95\%$ confidence interval (**Fig. 5g**).

45. Leivers, A.L. *et al.* Discovery of selective small molecule type iii phosphatidylinositol 4-kinase α (PI4KIIIα) inhibitors as anti hepatitis C (HCV) agents. *J. Med. Chem.* **57**, 2091–2106 (2014).
46. Oikawa, T. *et al.* Sal-like protein 4 (SALL4), a stem cell biomarker in liver cancers. *Hepatology* **57**, 1469–1483 (2013).
47. Schmelzer, E. *et al.* Human hepatic stem cells from fetal and postnatal donors. *J. Exp. Med.* **204**, 1973–1987 (2007).
48. Wang, Y. *et al.* Paracrine signals from mesenchymal cell populations govern the expansion and differentiation of human hepatic stem cells to adult liver fates. *Hepatology* **52**, 1443–1454 (2010).
49. Kubota, H. & Reid, L.M. Clonogenic hepatoblasts, common precursors for hepatocytic and biliary lineages, are lacking classical major histocompatibility complex class I antigen. *Proc. Natl. Acad. Sci. USA* **97**, 12132–12137 (2000).
50. Ma, Y., Yates, J., Liang, Y., Lemon, S.M. & Yi, M. NS3 helicase domains involved in infectious intracellular hepatitis C virus particle assembly. *J. Virol.* **82**, 7624–7639 (2008).
51. Yanagi, M., Purcell, R.H., Emerson, S.U. & Bukh, J. Transcripts from a single full-length cDNA clone of hepatitis C virus are infectious when directly transfected into the liver of a chimpanzee. *Proc. Natl. Acad. Sci. USA* **94**, 8738–8743 (1997).
52. Shimakami, T. *et al.* Stabilization of hepatitis C virus RNA by an Ago2–miR-122 complex. *Proc. Natl. Acad. Sci. USA* **109**, 941–946 (2012).
53. Date, T. *et al.* Novel cell culture-adapted genotype 2a hepatitis C virus infectious clone. *J. Virol.* **86**, 10805–10820 (2012).
54. Saeed, M. *et al.* Efficient replication of genotype 3a and 4a hepatitis C virus replicons in human hepatoma cells. *Antimicrob. Agents Chemother.* **56**, 5365–5373 (2012).
55. Timpe, J.M. *et al.* Hepatitis C virus cell-cell transmission in hepatoma cells in the presence of neutralizing antibodies. *Hepatology* **47**, 17–24 (2008).
56. Kannan, R.P., Hensley, L.L., Evers, L.E., Lemon, S.M. & McGivern, D.R. Hepatitis C virus infection causes cell cycle arrest at the level of initiation of mitosis. *J. Virol.* **85**, 7989–8001 (2011).
57. Puneet, P. *et al.* SphK1 regulates proinflammatory responses associated with endotoxin and polymicrobial sepsis. *Science* **328**, 1290–1294 (2010).
58. Dansako, H. *et al.* Class A scavenger receptor 1 (MSR1) restricts hepatitis C virus replication by mediating toll-like receptor 3 recognition of viral RNAs produced in neighboring cells. *PLoS Pathog.* **9**, e1003345 (2013).
59. Shaner, R.L. *et al.* Quantitative analysis of sphingolipids for lipidomics using triple quadrupole and quadrupole linear ion trap mass spectrometers. *J. Lipid Res.* **50**, 1692–1707 (2009).
60. Sullards, M.C., Liu, Y., Chen, Y. & Merrill, A.H. Jr. Analysis of mammalian sphingolipids by liquid chromatography tandem mass spectrometry (LC-MS/MS) and tissue imaging mass spectrometry (TIMS). *Biochim. Biophys. Acta* **1811**, 838–853 (2011).
61. Reynolds, E.S. The use of lead citrate at high pH as an electron-opaque stain in electron microscopy. *J. Cell Biol.* **17**, 208–212 (1963).
62. Papin, J.F., Vahrson, W. & Dittmer, D.P. SYBR green-based real-time quantitative PCR assay for detection of West Nile Virus circumvents false-negative results due to strain variability. *J. Clin. Microbiol.* **42**, 1511–1518 (2004).
63. Gurukumar, K.R. *et al.* Development of real time PCR for detection and quantitation of Dengue Viruses. *Virol. J.* **6**, 10 (2009).
64. Qu, L. *et al.* Disruption of TLR3 signaling due to cleavage of TRIF by the hepatitis A virus protease-polymerase processing intermediate, 3CD. *PLoS Pathog.* **7**, e1002169 (2011).
65. Ahmed, R., Salmi, A., Butler, L.D., Chiller, J.M. & Oldstone, M.B. Selection of genetic variants of lymphocytic choriomeningitis virus in spleens of persistently infected mice. Role in suppression of cytotoxic T lymphocyte response and viral persistence. *J. Exp. Med.* **160**, 521–540 (1984).
66. Bartenschlager, R., Lohmann, V. & Penin, F. The molecular and structural basis of advanced antiviral therapy for hepatitis C virus infection. *Nat. Rev. Microbiol.* **11**, 482–496 (2013).
67. Humphrey, W., Dalke, A. & Schulten, K. VMD: visual molecular dynamics. *J. Mol. Graph.* **14**, 33–38, 27–28 (1996).

JVI
Journals.ASM.org

hnRNP L and NF90 Interact with Hepatitis C Virus 5′-Terminal Untranslated RNA and Promote Efficient Replication

You Li, Takahiro Masaki, Tetsuro Shimakami,* Stanley M. Lemon

Departments of Medicine and Microbiology Immunology, and Lineberger Comprehensive Cancer Center, The University of North Carolina at Chapel Hill, Chapel Hill, North Carolina, USA

ABSTRACT

The 5′-terminal sequence of the hepatitis C virus (HCV) positive-strand RNA genome is essential for viral replication. Critical host factors, including a miR-122/Ago2 complex and poly(rC)-binding protein 2 (PCBP2), associate with this RNA segment. We used a biotinylated RNA pulldown approach to isolate host factors binding to the HCV 5′ terminal 47 nucleotides and, in addition to Ago2 and PCBP2, identified several novel proteins, including IGF2BP1, hnRNP L, DHX9, ADAR1, and NF90 (ILF3). PCBP2, IGF2BP1, and hnRNP L bound single-stranded RNA, while DHX9, ADAR1, and NF90 bound a cognate double-stranded RNA bait. PCBP2, IGF2BP1, and hnRNP L binding were blocked by preannealing the single-stranded RNA bait with miR-122, indicating that they bind the RNA in competition with miR-122. However, IGF2BP1 binding was also inhibited by high concentrations of heparin, suggesting that it bound the bait nonspecifically. Among these proteins, small interfering RNA-mediated depletion of hnRNP L and NF90 significantly impaired viral replication and reduced infectious virus yields without substantially affecting HCV internal ribosome entry site-mediated translation. hnRNP L and NF90 were found to associate with HCV RNA in infected cells and to coimmunoprecipitate with NS5A in an RNA-dependent manner. Both also associate with detergent-resistant membranes where viral replication complexes reside. We conclude that hnRNP and NF90 are important host factors for HCV replication, at least in cultured cells, and may be present in the replication complex.

IMPORTANCE

Although HCV replication has been intensively studied in many laboratories, many aspects of the viral life cycle remain obscure. Here, we use a novel RNA pulldown strategy coupled with mass spectrometry to identify host cell proteins that interact functionally with regulatory RNA elements located at the extreme 5′ end of the positive-strand RNA genome. We identify two, primarily nuclear RNA-binding proteins, hnRNP L and NF90, with previously unrecognized proviral roles in HCV replication. The data presented add to current understanding of the replication cycle of this pathogenic human virus.

Hepatitis C virus (HCV) is a leading cause of liver disease, including chronic hepatitis, cirrhosis, and hepatocellular carcinoma. It is classified within the *Flaviviridae* family of viruses and has a single-stranded, messenger-sense RNA genome ~9.7 kb in length. The replication of HCV viral RNA is uniquely dependent on a host-factor microRNA (miRNA), miR-122, which is highly abundant in liver (1, 2). There are two conserved miR-122 binding sites (S1 and S2) located near the 5′ end of the positive-sense HCV RNA genome. Direct interactions between miR-122, and these sites are essential for the HCV life cycle (3, 4). This is reflected clinically in dose-dependent reductions of circulating HCV RNA after intravenous administration of an antisense miR-122 "antagomir" to HCV-infected chimpanzees and humans (5, 6).

Previous studies demonstrate that binding of miR-122 to the 5′-untranslated region (5′UTR) of the HCV genome stimulates viral protein expression (7, 8) and also physically stabilizes the RNA in infected cells (9, 10). Similar to conventional miRNA action, miR-122 recruits Argonaute 2 protein (Ago2) to the viral RNA (9, 11). The stability conferred by the miR-122/Ago2 complex can be substituted functionally by addition of a 5′ cap, suggesting that it protects against 5′-exonuclease-mediated decay (9). Indeed, studies of RNA decay pathways have revealed that HCV RNA is primarily degraded from the 5′ end by the exonuclease Xrn1 in infected cells and that the binding of miR-122 to the HCV 5′UTR effectively blocks Xrn1-mediated degradation (10). However, depletion of Xrn1 in Huh-7.5 cells failed to rescue the replication of HCV RNA containing single-base substitutions in both S1 and S2 that ablate miR-122 binding, suggesting that miR-122 has an additional, essential role in HCV replication beyond protecting the RNA genome from Xrn1-mediated degradation (10).

The 5′UTR of HCV folds into conserved stem-loops (SL1 to SL4), with SL2 to SL4 participating in HCV internal ribosome entry site (IRES)-directed translation (12, 13). The 5′UTR serves as a platform to recruit proteins that are essential for viral protein synthesis and RNA replication. Cellular RNA-binding proteins, including eukaryotic initiation factor 3 (eIF3), the 40S ribosomal subunit, polypyrimidine-tract-binding protein (PTB), poly(rC)-binding protein 2 (PCBP2), and La autoantigen, have been shown to bind to the 5′UTR of HCV RNA and to play important roles in viral translation and/or replication (14–18). The miR-122 binding sites (S1 and S2) are located upstream of SL2, encompassing the

Received 23 January 2014 Accepted 6 April 2014
Published ahead of print 9 April 2014
Editor: B. Williams
Address correspondence to Stanley M. Lemon, smlemon@med.unc.edu.
* Present address: Tetsuro Shimakami, Department of Gastroenterology, Kanazawa University Graduate School of Medicine, Takara-Machi, Japan.

doi:10.1128/JVI.00225-14

SL1 region and extending to the very 5′ end of HCV RNA (Fig. 1A). This region has been shown to be essential for HCV RNA replication (14, 19). Two proteins, Ago2 and PCBP2, are known to associate with this region: Ago2 is recruited by miR-122, whereas PCBP2 has been suggested to bind to SL1, a small stem-loop near the 5′ end (9, 14, 20). In the present study, we sought to identify additional proteins associating with this region of the HCV genome, either dependently or independently of miR-122, and to assess their function in HCV replication. We found that hnRNP L and IGF2BP1 bind to single-stranded RNA (ssRNA) representing the extreme 5′ end of the HCV genome, whereas DHX9, ADAR1, and NF90 associate with the cognate double-stranded RNA (dsRNA). Among these proteins, hnRNP L and NF90 are shown to be required for efficient HCV replication but not HCV IRES-directed translation. Both proteins bind viral RNA in infected cells and may be associated with viral replication complexes.

MATERIALS AND METHODS

Cells, reagents, and plasmids. Huh-7.5 cells (obtained from Charles Rice, Rockefeller University) and FT3-7 cells were maintained as described previously (8, 21). U2OS cells with conditional expression of the HCV NS5A protein were kindly provided by Darius Moradpour (Université de Lausanne) (22). WST-1 reagent (Millipore) was used to monitor cell proliferation according to the manufacturer's suggested protocol. Plasmids pH77S.3/GLuc2A and pHJ3-5 (both infectious HCV molecular clones) have been described previously (8, 23). pHCVΔC-GLuc expresses an HCV "minigenome" comprised of RNA sequence encoding the first 12 amino acids of the HCV core protein fused at its downstream end to the *Gaussia princeps* luciferase (GLuc) sequence and flanked by the 5′ and 3′ untranslated RNA sequences of H77S, a genotype 1a virus (24).

RNA transcription. Viral RNAs were transcribed *in vitro* as described previously (9).

Biotinylated RNA pull-down. Oligoribonucleotide baits, H77S 1-47 and S1/S2p6 (Fig. 1A), representing the 5′ 47 nucleotides of wild-type genotype 1 HCV RNA and a related S1/S2p6 mutant (see below) and conjugated to biotin at their 3′ ends, were synthesized by Dharmacon (Pittsburgh, PA). These RNA baits (10 pmol in each reaction) were incubated alone or with 10 pmol of a similarly synthesized complementary antisense oligonucleotide (to generate a dsRNA bait) or variable amounts of single-strand synthetic miR-122 (9), heated at 75°C for 5 min, and then cooled to room temperature. Annealed RNAs were bound to magnetic streptavidin T1 beads (Invitrogen) according to the manufacturer's instructions and then incubated with Huh-7.5 cell cytoplasmic lysate for 1 h at 4°C. Anti-miR-122 or anti-random locked nucleic acid (LNA) oligonucleotides (9) were added to the lysate where indicated. Proteins bound to the beads were eluted with SDS-PAGE sample buffer, resolved by SDS-PAGE and subjected to SYPRO Ruby staining or immunoblotting with specific antibodies. Specific bands were cut from the gel and proteins in each identified by mass spectrometry with the UNC Proteomics Core Facility.

Transfections. siRNA pools targeting IGF2BP1, hnRNP L, ADAR1, DHX9, NF90, and control small interfering RNA (siRNA) pools (Dharmacon) were transfected using siLentfect lipid reagent (Bio-Rad). *In vitro*-transcribed HCV RNA (1.25 μg) was transfected into 2.5×10^6 Huh-7.5 cells using the TransIT mRNA kit (Mirus Bio).

Real-time reverse transcription-PCR (RT-PCR). To quantify HCV RNA, cDNA was produced by reverse transcription of RNA using oligo(dT) and an HCV-specific primer (5′-GGCCAGTATCAGCACTCTC TGCAGTC-3′) targeting the 3′UTR of the genome and SuperScript III reverse transcriptase (Invitrogen). Quantitative PCR analysis was carried out using iTaq SYBR green Supermix with the CFX96 system (Bio-Rad). HCV RNA abundance was determined by reference to a standard curve using PCR primers targeting the 5′UTR (5′-CATGGCGTTAGTATGAG TGTCGT-3′ and 5′-CCCTATCAGGCAGTACCACAA-3′) and normalized to the abundance of β-actin mRNA (primers 5′-GTCACCGGAGTC CATCACG-3′ and 5′-GACCCAGATCATGTTTGAGACC-3′). The HCV minigenome RNA was amplified by the primers 5′-CACGCCCAAGATG AAGAAGT-3′ and 5′-GAACCCAGGAATCTCAGGAATG-3′.

Immunoblots. Immunoblotting was carried out according to standard methods with the following antibodies: mouse monoclonal antibody (MAb) to β-actin (AC-74; Sigma-Aldrich); rat MAb to Ago2 (Sigma-Aldrich); rabbit polyclonal antibodies to ADAR1, NF90, and DHX9 (Bethyl Laboratory); mouse MAb to hnRNP L (Millipore); rabbit polyclonal antibody to IGF2BP1 (Abcam); mouse MAb to PCBP2 (Abnova); mouse MAb to hnRNP C and PTB (Abcam); MAb to HCV core protein (Pierce); and rabbit polyclonal antibody to HCV NS5A protein (kindly provided by Takaji Wakita). Protein bands were visualized with an Odyssey infrared imaging system (Li-Cor Biosciences).

***Gaussia* luciferase (GLuc) assay.** Cell culture supernatant fluids were collected at intervals after RNA transfection, and cells were refed with fresh media. Secreted GLuc activity was measured in the supernatant fluids using the Biolux *Gaussia* luciferase assay kit (New England BioLabs) as previously described (23).

Infectious virus titration. Supernatant fluids (100 μl) from HJ3-5 virus-infected cells were incubated with 5×10^4 uninfected Huh-7.5 cells in a 48-well plate for 6 h. After replacement of media, cells were allowed to grow for 72 h before fixation and immunolabeling with anti-core antibody (Pierce). Foci of infected cells were visualized and infectious virus titer quantified in terms of focus-forming units as described previously (24).

Preparation of cytoplasmic and nuclear lysates. Huh-7.5 cells were harvested in lysis buffer A (150 mM KCl, 25 mM Tris-HCl [pH 7.5], 5 mM EDTA,1% Triton X-100, 2 mM dithiothreitol, Complete protease inhibitor mixture [Roche, Mannheim, Germany]). Lysates were centrifuged for 5 min at 1,000 × *g* at 4°C. The supernatants were collected as a cytoplasmic lysate. The nuclear pellet was washed with phosphate-buffered saline and lysed in buffer B (500 mM KCl, 25 mM Tris-HCl [pH 7.5], 2 mM EDTA, 1% NP-40, 0.1% SDS, Complete protease inhibitor mixture). Cytoplasmic and nuclear lysates were cleared by centrifugation at 17,000 × *g* for 10 min at 4°C.

Immunoprecipitation. Cytoplasmic lysates of HJ3-5 virus-infected Huh-7.5 cells were incubated with anti-hnRNP L (Millipore), anti-NF90 (Bethyl Labs), anti-Dcp1a (Abnova), rabbit anti-NS5A (kindly provided by T. Wakita), or isotype control IgG at 4°C for 2 h, followed by addition of 30 μl of protein G-Sepharose (GE Healthcare) for 1 h. RNase A was added to the lysate where indicated. The Sepharose beads were washed three times in lysis buffer. Proteins were eluted with SDS-PAGE sample buffer and subjected to SDS-PAGE, followed by immunoblotting. Coprecipitated RNAs were extracted using the RNeasy minikit (Qiagen). HCV RNA was detected by reverse transcription-PCR (RT-PCR) using the SuperScript One-Step RT-PCR (Invitrogen) and the specific primers 5′-CA TGGCGTTAGTATGAGTGTCGT-3′ and 5′-CCCTATCAGGCAGTAC CACAA-3′.

Membrane flotation assay. The membrane flotation assay was carried out according the method of Okamoto et al. (25) with some modifications. Eight million FT3-7 cells with or without HJ3-5 virus infection were harvested, suspended in 1 ml of TNE buffer (25 mM Tris-HCl [pH 7.4] containing 150 mM NaCl, 5 mM EDTA, and Complete protease inhibitor cocktail), and then disrupted by 20 passages through a 25-gauge needle. After low-speed centrifugation (1,000 × *g*), postnuclear supernatants were divided into two tubes and incubated for 30 min on ice with or without 0.5% Triton X-100. The lysates were mixed with 1.2 ml of an iodixanol (OptiPREP; Sigma-Aldrich, St. Louis, MO) solution with a final concentration of 45%. This mixture was overlaid with a 35 to 10% iodixanol gradient and then centrifuged at 42,000 rpm and 4°C for 14 h in an SW55 Ti rotor (Beckman Coulter, Fullerton, CA). Twelve fractions were collected from the top of the gradient and precipitated with trichloroacetic acid, followed by acetone washing. Dried pellets were resolved in the loading buffer, boiled, and subjected to SDS-PAGE, followed by immu-

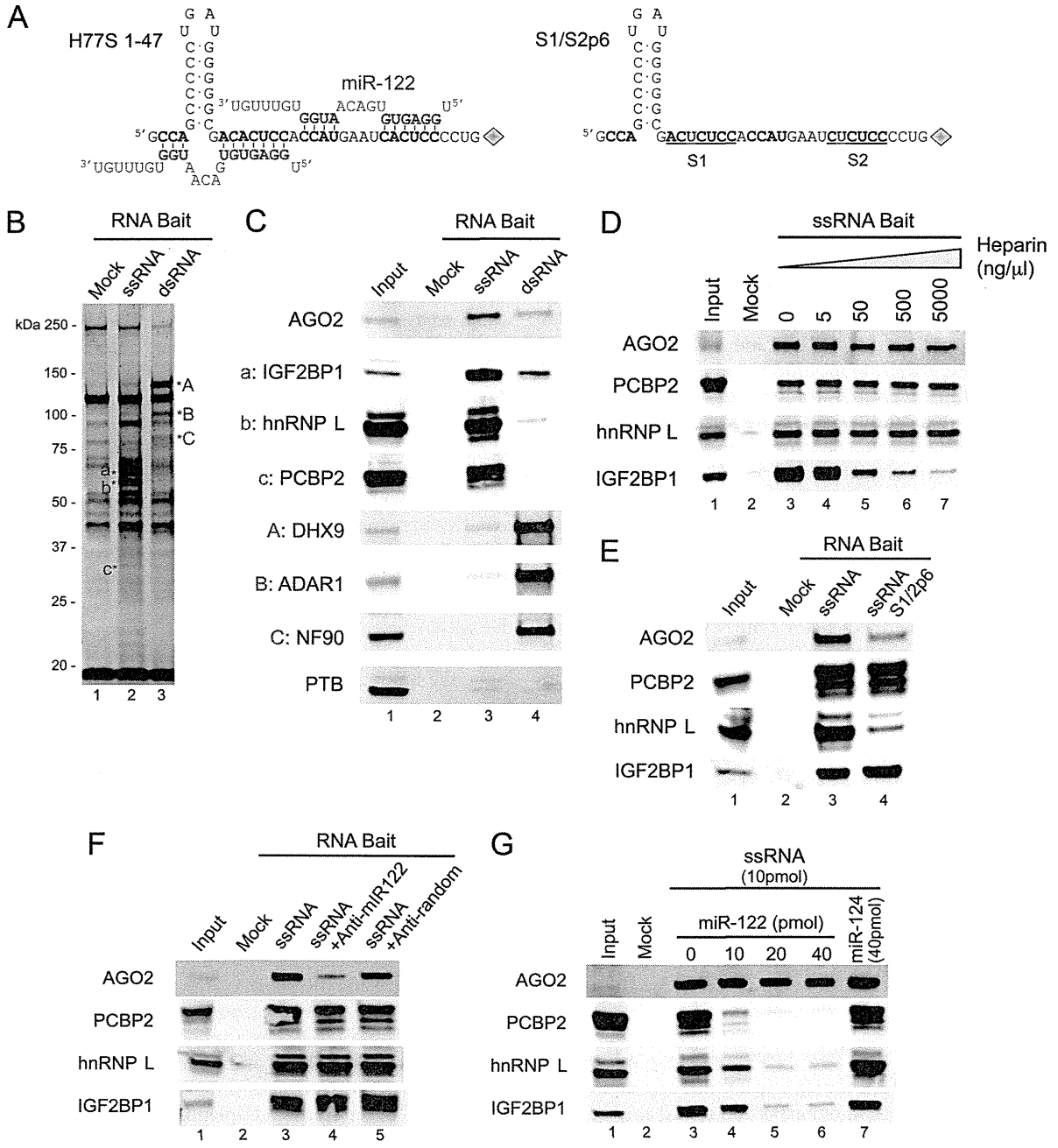

FIG 1 Identification of proteins binding to the 5′ end of the HCV 5′UTR. (A) RNA baits used in the pulldown experiments. (Left) ssRNA oligonucleotide representing the 5′ most 47 bases in the HCV genome (H77S virus, black font). Two copies of miR-122 (red font) are shown bound to the probe as determined by prior genetic studies (21). Positions involved in base-pairing are shown in boldface. (Right) S1/S2p6, a related bait with base substitutions (red font) at position 6 of the two miR-122 seed sequence binding sites, S1 and S2 (underlined). RNA probes were conjugated to biotin (diamond symbol) at their 3′ ends. (B) RNA pulldown. Synthetic biotinylated RNA bait (H77S 1-47) was incubated with Huh-7.5 cytoplasmic lysate by itself (ssRNA bait) or after being preannealed with a complementary negative-strand RNA (dsRNA bait). Proteins pulled down were resolved by SDS-PAGE and stained by SYPRO Ruby. Unique protein bands in each lane indicated by asterisks were identified by mass spectrometry. Mock, no RNA bait. (C) Protein samples from panel B were subjected to immunoblot analysis with specific antibodies. 2% input lysate was loaded as reference. Ago2, IGF2BP1, hnRNP L and PCBP2 bind preferentially to ssRNA bait, while DHX9, ADAR1, and NF90 bind to dsRNA bait. PTB was detected as a negative control. (D) RNA pulldown assay was done as in panel B using ssRNA bait in the presence of the indicated amount of heparin. Ago2, PCBP2, IGF2BP1, and hnRNP L proteins were detected by immunoblotting. Heparin inhibited the binding of IGF2BP1, but not the other proteins. (E) RNA pulldown assay was performed as in panel B using RNA bait containing single mutations in S1 and S2 site (S1/2p6, see panel A). S1/S2p6 RNA demonstrated reduced binding of Ago2 and hnRNP L but not IGF2BP1 and PCBP2. (F) RNA pulldown assay was carried out as in panel B except that anti-miR-122 or anti-random oligonucleotides were added to the lysate. Ago2, PCBP2, IGF2BP1, and hnRNP L proteins were detected by immunoblotting. Anti-miR-122 blocked the binding of Ago2 but not the other proteins. (G) RNA pulldown assay was carried out as in panel B except that 10 pmol of ssRNA bait was preannealed with the indicated amount of single-strand miR-122 or miR-124. Ago2, PCBP2, IGF2BP1, and hnRNP L proteins were detected by immunoblotting. The addition of miR-122 blocked the binding of PCBP2, IGF2BP1, and hnRNP L but not Ago2.

noblotting. Protease treatment was carried out with 1 μg of proteinase K per 50-μl fraction sample with or without 1% NP-40 and then incubated at 37°C for 30 min.

Statistical tests. Statistical significance was calculated using Prism 5 for Mac OS X (GraphPad Software, Inc.) and specific statistical tests as indicated.

RESULTS

To identify proteins that bind to the 5′ terminus of positive-strand HCV RNA, we used a biotin-tagged RNA pulldown strategy. A synthetic oligonucleotide representing the 5′ 47 nucleotides of genotype 1 H77 virus was conjugated to biotin at its 3′ end (Fig. 1A, left). This RNA bait (ssRNA bait) was incubated with Huh-7.5 cell cytoplasmic lysate. Since double-strand RNA is an important intermediate in HCV RNA replication, we also sought to isolate proteins that bind to a double-stranded version of this bait by preannealing it with a complementary negative-strand RNA oligonucleotide (dsRNA bait). The proteins associated with these baits were pulled down with streptavidin beads, resolved by SDS-PAGE, and visualized by SYPRO Ruby staining (Fig. 1B). Specific bands that were pulled down by ssRNA or dsRNA bait were cut from the gel and identified by mass spectrometry. We identified three proteins that specifically associated with the ssRNA bait (Fig. 1B, lane 2, bands a, b, and c). These were identified by mass spectrometry as insulin-like growth factor 2 mRNA binding protein 1 (IGF2BP1), heterogeneous nuclear ribonucleoprotein L (hnRNP L), and PCBP2, respectively. Three bands that specifically bound the dsRNA bait (Fig. 1B, lane 3, bands A, B, and C) were found to be DEAH box helicase 9 (DHX9, also known as ATP-dependent RNA helicase 9), dsRNA-specific adenosine deaminase (ADAR1), and "nuclear factor of activated T cells 90 kDa" (NF90; also known as interleukin enhancer-binding factor 3 [ILF3]). To confirm the mass spectrometry results, we used immunoblotting with specific antibodies to these proteins. Consistently, we detected specific binding of IGF2BP1, hnRNP L, and PCBP2 to the ssRNA bait and binding of DHX9, ADAR1, and NF90 to the dsRNA bait (Fig. 1C).

As the 5′ HCV RNA sequence contains both miR-122 binding sites, we anticipated that endogenous miR-122 would bind with Ago2 protein to the ssRNA bait (9). This was confirmed in immunoblots (Fig. 1C), although Ago2 was not visible by SYPRO Ruby staining due to low abundance or inefficient binding of endogenous miR-122 to the bait. In contrast, PTB, an RNA-binding protein required for HCV replication (16), did not appear to bind either ssRNA or dsRNA bait in our assay and served as a negative control (Fig. 1C). IGF2BP1, hnRNP L, and PCBP2 are all RNA-binding proteins. PCBP2 has been shown to bind to the SLI region of the HCV 5′UTR and to be required for HCV replication (14, 20). IGF2BP1 has also been found to bind to the 5′ sequence of HCV RNA and to modulate HCV IRES function (26, 27). hnRNP L is a novel factor identified in our assay that has not been shown previously to bind the 5′ end of HCV RNA. DHX9, ADAR1, and NF90 all contain double-strand RNA-binding motifs, which is consistent with their binding to the dsRNA bait. DHX9 has RNA helicase activity, ADAR1 is an RNA specific adenosine deaminase, and NF90 was first discovered as a subunit of a nuclear transcription factor complex (28). Their function in HCV replication has not been well studied. To test the specificity of the interaction between these RNA-binding proteins and the bait, we repeated the ssRNA pulldown assay in the presence of a nonspecific competitor, heparin (Fig. 1D). Increasing amounts of heparin reduced the binding of IGF2BP1 but had little effect on the binding of Ago2, PCBP2, or hnRNP L, confirming that Ago2 (miR-122), PCBP2 and hnRNP L interact with the HCV 5′ terminal sequence in a specific and likely sequence-dependent manner.

To determine whether the binding of IGF2BP1, hnRNP L, and PCBP2 to the HCV 5′ sequence is dependent on binding of miR-122, such as Ago2 (9), we repeated the pulldown assay using a mutant RNA bait that contains a single base substitution in both the S1 and the S2 sites (Fig. 1A, right, S1/2p6) that significantly reduces miR-122 binding. As expected (9), the mutation substantially reduced Ago2 binding (Fig. 1E). Interestingly, it also diminished binding of hnRNP L but not PCBP2 or IGF2BP1 (Fig. 1E), which suggests that hnRNP L binding might be dependent on miR-122. To assess this further, we carried out a pulldown assay in the presence of an antisense anti-miR-122 locked nucleic acid (LNA) oligonucleotide. However, while the antagomir dramatically reduced Ago2 binding to the ssRNA bait, there was no effect on the binding of any of the other proteins, indicating that they bind to HCV RNA independently of miR-122 (Fig. 1F). Therefore, the reduced binding of hnRNP L to the p6 mutant RNA is unlikely to be due to reduced miR-122 binding and is more likely caused by direct disruption of the hnRNP L binding site. If this is the case, it indicates that hnRNP L binds to the same or overlapping site as the miR-122 seed sequence. Indeed, when we preannealed miR-122 to the ssRNA bait, the binding of hnRNP L was dramatically decreased in a miR-122 dose-dependent manner (Fig. 1G). Surprisingly, the binding of IGF2BP1 and PCBP2 was also blocked by miR-122. These data indicate that IGF2BP1, hnRNP L, and PCBP2 bind the HCV 5′ sequence in competition, not in cooperation with miR-122. This is not surprising given the extensive interactions of miR-122 with this segment of the viral genome (Fig. 1A, left).

We next sought to determine whether proteins that bind the 5′ end of HCV RNA have a function in HCV replication. Since Ago2 and PCBP2 have already been demonstrated to be required for HCV replication, we focused on the other proteins detected in our pulldown assay, including IGF2BP1, hnRNP L, ADAR1, DHX9, and NF90. We knocked down the expression of these proteins by transfecting specific siRNAs into Huh-7.5 cells (Fig. 2A) and then transfected a modified HCV genomic RNA that expresses *Gaussia princeps* luciferase (GLuc) as a reporter. Secreted GLuc activity was monitored over 72 h as an indicator of HCV replication (9). siRNA-mediated depletion of hnRNP L and NF90 substantially reduced HCV replication. Depletion of IGF2BP1 and DHX9 caused much smaller but nonetheless reproducible and statistically significant reductions in replication, while ADAR depletion was without effect (Fig. 2B). These results suggested that, among these RNA-binding proteins, hnRNP L and NF90 may be particularly important for efficient HCV replication. However, depletion of either protein also caused significant defects in cell proliferation as measured by WST-1 assay, in both cases reducing cell growth by ca. 25% (Fig. 2C).

Further studies focused on hnRNP L and NF90. To minimize the impact of their depletion on cell growth, we repeated the RNA interference experiments in cells cultured in media containing 2% serum (Fig. 3). HCV replication was significantly reduced by depletion of either protein, as measured by GLuc activity (Fig. 3A). Total HCV RNA abundance was also reduced by ca. 60%, after hnRNP L depletion and 40% after NF90 depletion (Fig. 3B). Importantly, hnRNP L and NF90 depletion resulted in little change